

## Highlights

### A test of meta-heuristic algorithms for parameter extraction of next-generation solar cells with S-shaped current-voltage curves

Oleg Olikh

- 14 meta-heuristic algorithms are used to parameter estimation from S-shaped *IV* curves
- The algorithms' efficiencies are compared by using nonparametric statistic methods
- The relevance of using the square error fitness function has been demonstrated
- STLBO and ADELI excel in identifying parameters of the opposed two-diode model

# A test of meta-heuristic algorithms for parameter extraction of next-generation solar cells with S-shaped current-voltage curves

Oleg Olikh

Taras Shevchenko National University of Kyiv, 64/13, Volodymyrska Street, Kyiv, 01601, Ukraine

---

## ARTICLE INFO

**Keywords:**

- S-shaped *IV* characteristics
- Opposed two-diode model
- Parameter estimation
- Meta-heuristic algorithms
- Nonparametric statistical procedure
- Solar cell models

---

## ABSTRACT

Identifying parameters of photovoltaic (PV) models based on measured current-voltage (*IV*) characteristic curves is critical for simulating, evaluating, and controlling PV systems. *IV* characteristics of the latest-generation solar cells (SCs) often display an S-shaped deformation. In this paper, we explore the potential of meta-heuristic algorithms to address the parameter estimation problems associated with PV cells that exhibit S-shaped *IV* characteristics. This estimation is performed within the framework of the opposed two-diode model. We implemented a total of 14 algorithms from various classes to extract the SC parameters from synthetic *IV* curves, which were generated using a range of parameter values. The results were compared by using nonparametric statistical methods. These methods include the Wilcoxon signed-rank test for pairwise comparisons, and the Friedman, Friedman Aligned, and Quade tests for multiple comparisons. Comprehensive results and analyses show that the STLBO (Simplified teaching-learning based optimization algorithm) and ADELI (Adaptive differential evolution with the Lagrange interpolation argument) algorithms demonstrate highly competitive performance in terms of accuracy and reliability. This paper underscores the efficacy of advanced meta-heuristic algorithms in solving complex non-linear optimization problems in the domain of photovoltaic research, particularly concerning the unique challenges posed by S-shaped *IV* characteristics of new-generation solar cells.

---

## 1. Introduction

The intensive use of fossil fuels has led to numerous ecological and energy-related challenges for humanity. Addressing these issues, the most hopeful solution appears to be the adoption of renewable green energy sources. However, this requires tackling several key tasks, the primary among them being the direct generation of energy and the ability to store it to ensure a reliable supply. Whereas the latter can be addressed through the development of energy storage devices (such as lithium-ion batteries or next-generation dual-ion batteries [1, 2, 3]), photovoltaics (PV) is widely regarded as the most promising clean technology for energy-producing to meet the escalating energy demands of Earth's population. According to the International Energy Agency reports, the cumulative installed PV capacity was forecasted to rise to 1.826 TW by 2026 and 14.5 TW by 2050 [4].

One of the most common approaches to understanding the electrical characteristics of PV devices is the use of an equivalent circuit model. Such lumped-parameter modeling enables simulation, analysis, and optimization of device performance. Currently, silicon solar cells (Si-SCs) comprise approximately 90% of the global PV production capacity. For describing the operation of these conventional SCs, the following models are most widely utilized: single-diode model (SDM), double-diode model (DDM), and three-diode model (TDM). These models incorporate parallel-connected diodes that activate unidirectionally, a photo-current source, a parallel shunt resistance, and a series resistance. The PV module model (PVMM) is based on the SDM and consists of multiple diodes connected in series and/or parallel. In addition to developing these models, identifying the relevant parameters from current-voltage (*IV*) characteristics is a crucial task.

One prevalent approach for addressing such issues is the utilization of meta-heuristic algorithms. Numerous studies have been undertaken to compare the efficiency of meta-heuristic algorithms for parameter estimation under conventional SC models. Some research studies have focused on a single model, such as SDM [5], DDM [6, 7], or TDM

---

 [olegolikh@knu.ua](mailto:olegolikh@knu.ua) (Oleg Olikh)  
ORCID(s): 0000-0003-0633-5429 (Oleg Olikh)

[8], while others have examined both SDM and DDM simultaneously [9, 10, 11, 12]. Additionally, several publications have investigated the efficiency of algorithms in processing *IV* curves according to three different models: SDM, DDM, and PVMM [13, 14, 15, 16], or SDM, DDM, and TDM [17]. A comprehensive survey of meta-heuristic algorithms used for parameter extraction of conventional PV models can be found in the literature [18, 19]. Furthermore, the use of conventional SC models for testing newly developed algorithms is one of the most common approaches, following the utilization of benchmark functions from the Congress on Evolutionary Computation. The diversity of algorithms employed in analyzing conventional models is linked to the No Free Lunch (NFL) theorem [20]. NFL theorem states that no single algorithm can solve all optimization tasks effectively. Consequently, each problem, including the parameter estimation for every equivalent model, requires the selection of a distinct algorithm.

Recently, there has been intensive research focused on innovative developments, further experiments, and practical PV applications of various new-generation solar cells (NG-SCs). The operating principle of NG-SCs is qualitatively similar to that of Si-SCs, but the fourth quadrant of their *IV* characteristics often exhibits an S-shaped kink. The origin of the kink has been attributed to various physical phenomena, and this *IV* characteristics feature is typical among the most promising candidates for NG-SCs. Specifically, S-shaped *IV* curves have been observed in silicon heterojunction SCs [21], thin-film SCs such as CdTe, CI(G)S, and amorphous silicon PV devices [21, 22], normal and inverted organic SCs [23, 24, 25], perovskite SCs [21, 26], quantum dot SCs [27, 28], as well as in hybrid SCs [29, 30, 31]. Unfortunately, the conventional models have failed to describe the S-shaped kink adequately. Consequently, new models have been proposed to provide reasonable explanations for the shape of the *IV* curves from an electrical perspective. However, the NFL theorem suggests that algorithms that have demonstrated exceptional results for silicon solar cell models may not yield the same level of effectiveness for NG-SC models. Thus, the relevant task arises of selecting appropriate meta-heuristic algorithms for extracting parameters from the S-shaped *IV* curves. Certainly, meta-heuristic algorithms have been utilized in processing experimental S-shaped *IV* curves [32]. Nevertheless, to our knowledge, studies aimed at identifying the most optimal approach for solving these problems are currently lacking.

This study aimed to compare the effectiveness of meta-heuristic algorithms in extracting the parameters of NG-SCs from the S-shaped *IV* curves and to determine the most suitable ones for addressing this optimization problem. The parameters extraction has been done according to the De Castro two-diode model based on synthetic *IV* characteristics. The peculiarities of the De Castro model compared to others proposed for describing S-shaped curves, as well as the rationale for its selection, are detailed in Subsection 2.1. Subsection 2.2 deals with the procedure for generating synthetic *IV* curves. The investigation focused on 14 metaheuristic algorithms, briefly outlined in Subsection 2.3. Some of these algorithms have been well-known for a long time and have proven their effectiveness in solving a wide range of problems. Other algorithms are more recent and have been developed using the knowledge gained from their predecessors. When comparing the efficiency of algorithms, considerations were taken into account for computation speed, accuracy of parameter determination, and result repeatability. The comparison was carried out using various nonparametric statistical methods. The specific comparison criteria and nonparametric methods utilized are detailed in Subsection 2.4. The results of both pairwise and multiple comparisons are detailed in Section 3. Finally, we conclude this paper in Section 4.

## 2. Problem definition

### 2.1. Opposed two-diode model

Today, a considerable number of models have been proposed with the aim of explaining S-shaped *IV* curves. One of the earliest attempts was proposed by Mazhari [33]. This model is essentially a simplified version of the SDM, achieved by excluding resistances and incorporating an additional diode. But Mazhari's model fails to capture the linear-like rise of the S-shaped kink in the third quadrant. An improved model, which incorporates two resistances, was proposed for organic SCs [34]. Gaur and Kumar [23] offered equivalent model to represent the behavior of polymer SC in the dark. This model is almost identical to the DDM, except that one of the diodes has the opposite polarity. Another approach to developing equivalent models involves using multiple series-connected diodes. Zuo *et al.* [35] proposed a model consisting of two series-connected diodes in the same direction, two shunt resistors, and one series resistor. Another equivalent circuit holds two opposed diodes, two opposed current sources, and no resistors [27]. De Castro *et al.* [36] proposed a model consisting of two opposed diodes with shunt resistance for each, a series resistance, and a photo-current source — see Fig. 1. Further modifications to this model include adding a third diode that would either replace one of the shunt resistances [37] or be placed in parallel [38, 22]. In general, the development of models to describe S-shaped *IV* curves continues. For instance, a relatively recent proposal is the B2BDM model [39]. This

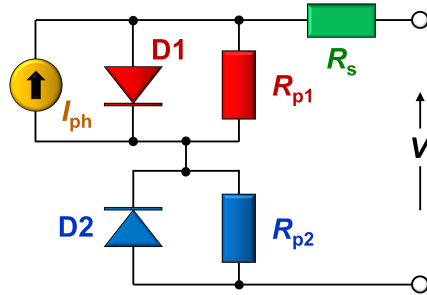


**Figure 1:** The opposed two-diode equivalent-circuit model of a solar cell [36].

model includes back-to-back diodes parallel with a shunt resistor and the photo-current source, all in series with an offset voltage source. This assembly is then connected in parallel to another diode and shunt resistor, again in series with a resistor. Some review about models for PV devices with S-shaped IV curves can be found in [40, 41].

Our study focused on the opposed two-diode model, proposed by De Castro [36]. This model represents a significant advancement as it successfully reproduces the S-shaped kink in the power-producing fourth quadrant of the illuminated *IV* characteristics. However, it encounters difficulties in accurately describing the *IV* curve beyond the open-circuit point in the first quadrant. Despite this drawback, the model is gaining attention for deriving analytical solutions of equivalent circuits [28] and is widely used to describe experimental *IV* curves of SCs with different structures [42, 32, 43, 44, 45, 46, 47, 48, 49]. In particular, these include polymer [46] and polymer/fullerene [44] bulk heterojunction photocells, ternary organic solar cells [47], and other types of organic structures [32, 43], perovskite solar cells with fullerene transport layer and carbon nanotube electrode [49], and perovskite solar cells with ionic liquid gating [48]. The popularity of the De Castro model is also because, in experiments, *IV* curves are typically measured only in the fourth quadrant from short-circuit current to open-circuit voltage. Therefore, our selection of the two-diode model is based on its universality and widespread applicability.

It can be seen from the model structure, as shown in Fig. 1, that some elements are identical to SDM. It is a current source accompanied by a diode D1, a shunt resistor  $R_{p1}$  to represent the leakage current, and a series resistor  $R_s$  to account for the losses associated with the load current. However, SDM fails to describe the S-shaped kink, which requires additional elements. As a result, a second diode (D2) and a second parallel resistor ( $R_{p2}$ ) are used. D2 is placed opposite D1 and represents the effect of traps at the active layer/cathode interface [36].

The analytical solution  $V(I)$  of the opposed two-diode equivalent circuit model is as follows [50, 51]:

$$V(I) = IR_s + \frac{n_1 kT}{q} g(x_1) - \frac{n_2 kT}{q} g(x_2) - \frac{n_1 kT}{q} \ln \left[ \frac{qI_{01}R_{p1}}{n_1 kT} \right] + \frac{n_2 kT}{q} \ln \left[ \frac{qI_{02}R_{p2}}{n_2 kT} \right], \quad (1)$$

with

$$x_1 = \ln \left( \frac{qI_{01}R_{p1}}{n_1 kT} \right) + \frac{q(I + I_{ph} + I_{01})R_{p1}}{n_1 kT}, \quad x_2 = \ln \left( \frac{qI_{02}R_{p2}}{n_2 kT} \right) - \frac{q(I - I_{02})R_{p2}}{n_2 kT}, \quad (2)$$

where  $g(x) = \ln(W(\exp(x)))$ ,  $W$  is the Lambert function [52],  $I_{01}$  and  $I_{02}$  are the saturation currents and  $n_1$  and  $n_2$  are the ideality factors for D1 and D2, respectively, and  $I_{ph}$  is the ideal photocurrent. Thus, the model employs eight lumped parameters ( $I_{01}$ ,  $n_1$ ,  $R_{p1}$ ,  $I_{02}$ ,  $n_2$ ,  $R_{p2}$ ,  $R_s$ , and  $I_{ph}$ ) that need to be determined from the *IV* curve. Thus, from an optimization perspective, the dimension of the problem is  $D = 8$ .

We used Eqs. (1)–(2) for initial simulating *IV* curves and during the subsequent fitting *IV* curves procedure with the help of meta-heuristic algorithms. The  $g$ -function was evaluated using an iterative procedure [51].

## 2.2. Synthetic IV curves

The research involved estimating the SC parameters from synthetic *IV* characteristics simulated using the opposed two-diode model. This approach enables us to assess the accuracy of the optimization meta-heuristic methods used, as the simulation was performed using known parameter values.

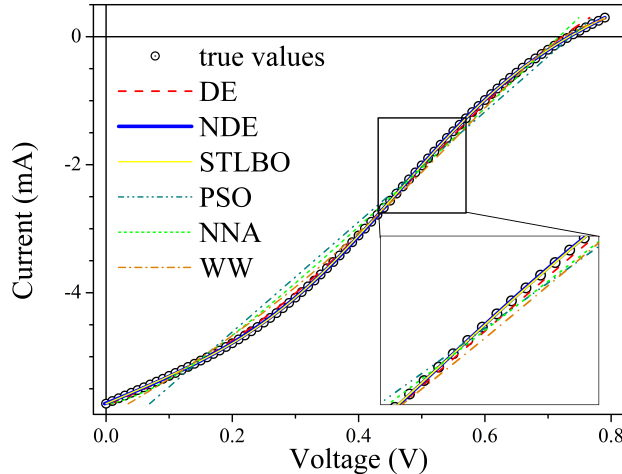


**Figure 2:** The current-voltage characteristic, which used in single-IV case (symbols). The values from Eq. (3) were assumed during the simulation. The fitting results of various meta—heuristic algorithms are represented by lines.

In the first part of the study, the performance of meta—heuristic algorithms for parameter estimation was evaluated using a single *IV* curve. This curve represents the experimental data of bulk heterojunction photocells prepared using a composite of *p*-DTS(FBTTh<sub>2</sub>)<sub>2</sub> and neat C<sub>70</sub> [46]. In this case (referred to below as the “Single-IV case”), meta—heuristic algorithms were primarily evaluated through a one-time application. Additionally, the appropriateness of using two different fitness functions was examined. In the second part, we simulated a set of *IV* characteristics and evaluated the average performance metrics of various algorithms. These curves correspond to the temperature range from 260 K to 350 K. The simulation took into account the temperature dependencies of parameters, closely resembling real SCs. From now on, this case will be referred to as the “IV-set case”. The precise parameter values used in the simulation are listed below.

### 2.2.1. Single-IV case

Previous studies [46, 53] have shown that the nonlinear least squares method (NLSM) can be used to fit experimental data from an organic SC, based on the opposed two-diode model, with minimal fitting error. However, the parameter values obtained from the same *IV* curve with repeated applications of NLSM may differ significantly. Hence, this approach fails to differentiate between similar *IV* curves derived from SCs with varying parameters.

To overcome this issue, Tada [53] successfully employed Bayesian estimation of parameters. To assess the capabilities of meta—heuristic methods in overcoming similar challenges, they were applied to an *IV* curve corresponding to such a problematic case. The parameter values were taken from [53]:

$$\begin{aligned} I_{01} &= 1.6 \cdot 10^{-6} \text{ mA}, & n_1 &= 1.92, & R_{p1} &= 190 \Omega, & I_{02} &= 0.16 \text{ mA}, \\ n_2 &= 1.92, & R_{p2} &= 190 \Omega, & R_s &= 45 \Omega, & I_{ph} &= 8 \text{ mA}. \end{aligned} \quad (3)$$

The *IV* curve was simulated using Eqs. (1)–(2) over a voltage range of 0–0.8 V with a 10 mV step at  $T = 300$  K. The simulation result is presented on Fig. 2 by symbols.

### 2.2.2. IV-set case

Employing various meta—heuristic algorithms to analyze a single *IV* curve is insufficient for gaining comprehensive insights into the efficacy of these methods in parameter estimation. Furthermore, the accuracy of parameter determination is closely tied to their exact values. For example, an increase in the  $R_p$  value can create challenges in accurately estimating resistance because the shunt will have a reduced impact on the overall shape of the *IV* curve. Additionally, the ratio between the parameter values is also crucial.

To test the methods across different parameter values, we generated synthetic data within a temperature range of 260 K to 350 K. In the simulation process, we considered the temperature dependencies of the parameters. We based our approach on known physical mechanisms of current flow in NG-SCs and used the reported temperature

dependencies of saturation current, ideality factor, shunt resistance, and series resistance. However, the main focus was on achieving a diversity of parameter ratios rather than attempting to precisely replicate real-life PV converters of a specific type. Furthermore, an S-shaped *IV* curve is observed in various types of solar cells, and diverse charge transport mechanisms significantly complicate the selection of a single possible temperature dependence for each of the eight model parameters.

Therefore, we assumed that the current conduction mechanism through D1 is close to tunneling. Hence,  $I_{01}$ ,  $R_{p1}$ , and  $(n_1 kT)$  remain constant with the selected values  $I_{01} = 0.015 \text{ mA}$ ,  $R_{p1} = 10^4 \Omega$ ,  $n_1 kT = 7 \text{ eV}$ . In the case of D2, the thermionic emission current was suggested, and  $I_{02}$  and  $n_2$  increased and decreased, respectively, with rising temperature [54]:

$$I_{02} = I_{002} \exp(-E_I/kT), \quad (4)$$

$$n_2 = 1 + T^*/T, \quad (5)$$

where  $I_{002}$ ,  $E_I$ , and  $T^*$  are the constants which are independent of temperature. The values of  $I_{002} = 500 \text{ A}$ ,  $E_I = 0.40 \text{ eV}$ , and  $T^* = 500 \text{ K}$  were used. For  $R_{p2}$ , an exponential temperature dependence was used, as it is commonly observed [55] in NG-SCs for shunt resistance:

$$R_{p2} = R_{p20} \exp(E_R/kT) \quad (6)$$

with  $R_{p20} = 9 \text{ m}\Omega$ ,  $E_R = 0.32 \text{ eV}$ . The linear temperature dependencies is expected for both  $I_{ph}$  [56, 57] and  $R_s$  [58, 59]:

$$y = y_0[1 - \text{TC}_y(T - 300)], \quad (7)$$

where  $y = I_{ph}$  or  $R_s$ ,  $y_0$  is the parameter value at room temperature,  $\text{TC}_y$  is the temperature coefficient of parameter. For most types of monocrystalline silicon solar cells, the  $\text{TC}_{I_{ph}}$  typically ranges from around  $-0.0004 \text{ K}^{-1}$  [60]. However, as the base thickness decreases, the temperature coefficient can increase to  $-0.0014 \text{ K}^{-1}$  [61]. For hydrogenated amorphous silicon solar cells,  $\text{TC}_{I_{ph}}$  is equal to  $-10^{-3} \text{ K}^{-1}$  [62]. For organic solar cells, the temperature coefficient can reach a magnitude of  $-0.003 \text{ K}^{-1}$  [63]. During the simulation, we assumed  $\text{TC}_{I_{ph}} = -10^{-3} \text{ K}^{-1}$ . Furthermore, the values of  $I_{ph0} = 1 \text{ mA}$ ,  $\text{TC}_{R_s} = 0.02 \text{ K}^{-1}$ , and  $R_{s0} = 50 \Omega$  were used.

The set of *IV* data consisted of 10 curves, simulated at 10 K intervals from 260 K to 350 K; in this case,  $n_1$ ,  $I_{02}$ ,  $n_2$ ,  $R_{p2}$ ,  $R_s$ , and  $I_{ph}$  varied from 6.37 to 4.73, from 9 to 880  $\mu\text{A}$ , from 2.92 to 2.43, from  $1.4 \cdot 10^4$  to 360  $\Omega$ , from 10 to 100  $\Omega$ , and from 0.96 to 1.05 mA, respectively. The *IV* curves were simulated over a voltage range of 0-1.0 V with a 10 mV step. The simulation results are depicted in Fig. 3 using symbols.

### 2.3. Meta-heuristic algorithms

In the literature, meta-heuristics are frequently categorized based on their sources of inspiration. This categorization involves blending true simulations with stochastic elements to mimic various biological behaviors, natural phenomena, and human behavior characteristics.

On this basis, any meta-heuristic algorithm can fall into one of the following main classes [64, 65, 66]: evolution-based methods (emulate the principles of evolutionary behavior observed in creatures in nature by relying on the concept of survival of the fittest), swarm intelligence-based methods (simulate the collective, dynamic, intelligent, and concerted gregarious conduct of collections of flocks or communities found in nature), bio-based methods (use biological processes unrelated to group behavior), chemical & physical-based methods (originate from the physical phenomena or chemical laws that exist in the universe), human-society-based methods (inspired by human beings, including various activities such as thinking and social behavior), and math-based methods (borrow the mathematical functions). Generally, there are hundreds of meta-heuristic optimization methods available. While we acknowledge that our selection may not be fully comprehensive, we utilized 14 methods, representing all classes mentioned above, to tackle the parameter estimation task within the framework of the opposed two-diode model for a solar cell. Hereafter, we will briefly describe each method and the parameters used during the fitting process.

*Differential evolution (DE).* DE is one of the classical methods, and it is based on the natural selection law, utilizing randomly generated initial populations, differential mutation, and probability crossover [67]. We used a penalty function recommended by Ishaque *et al.* [68] during the implementation process. According to Wang and

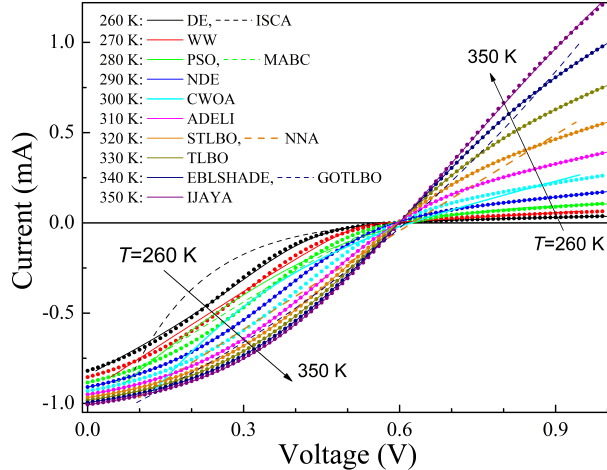


**Figure 3:** The current-voltage characteristics, which used in /V-set case (symbols). The values from ec. 2.2.2 were assumed during the simulation. The fitting results of various meta—heuristic algorithms are represented by lines.

Ye [67], this work used the following values: mutation scaling factor  $F = 0.8$ , crossover rate  $Cr = 0.3$ , and population size  $Np = 8 \times D = 64$ .

**Adaptive differential evolution with the Lagrange interpolation argument (ADELI).** This improved version of DE incorporates three main elements: local search using Lagrange interpolation, self-adaptive DE control parameter settings, and an adaptive mutational strategy [69]. The first element involves interpolating three potential solutions using a polynomial function to calculate the local minimum value. The self-adaptive control parameter settings include randomly altering the scaling factor and crossover rate values in each iteration. The adaptive mutational strategy determines the probability of employing Lagrange interpolation in each generation based on the best fitness function value. These incorporations aim to enhance exploitation capability and speed up the convergence. We used parameter values recommended by Huang *et al.* [69] during the implementation process. Additionally, we set  $Np$  to 64 for our numerical experiments.

**Differential evolution with neighborhood-based adaptive evolution mechanism (NDE).** The method employs a mutation strategy that considers neighborhood and individual information, along with an adaptive evolutionary mechanism [70].  $F$  and  $Cr$  values are determined using a weighted adaptive procedure [71]. The population size is adjusted adaptively using a simple reduction method from  $10 \times D = 80$  to 5.

**Success history based DE with hybridization mutation strategies and population size reduction (EBLSHADE).** The method represents a hybridization framework between the *pbest* and *ord\_pbest* mutation strategies. It stores a set of  $Cr$  and  $F$  values that have shown good performance in the recent past [72]. A linear  $Np$  reduction (from  $18 \times D = 144$  to 4) is used as well.

**Particle swarm optimization (PSO).** It is another classic method based on observations of the social behavior of animals, such as bird flocking, fish schooling, and swarm theory. According to Ye *et al.* [73], the values of learning factors  $l_1 = l_2 = 2$ , the final weight and the initial weight  $w_{max} = 0.9$ ,  $w_{min} = 0.4$ , and  $Np = 15 \times D = 120$  are used in this work.

The **modified artificial bee colony (MABC)** algorithm is inspired by the intelligent foraging behavior of honey bee swarms [74]. The control parameters include the population size ( $Np = 8 \times D = 64$ ) and the maximum number of generations, ( $L_{limit} = 36$ ), after which each non-improved food source is discarded.

**Chaotic Whale Optimization Algorithm (CWOA).** Initial algorithm (WOA) draws inspiration from the hunting behavior of humpback whales [75]. Whereas CWOA employs chaotic maps to compute and dynamically adjust its internal parameters [76]. In our study, we utilized the Singer chaotic map and set  $Np = 100$  to identify the SC parameters.

The **neural network algorithm (NNA)** is a meta—heuristic method inspired by both biological nervous systems and artificial neural networks [77]. In our paper, we used the recommended [77] value of  $Np = 50$ .

The *teaching learning based optimization (TLBO)* algorithm utilizes the idea of knowledge transfer within a classroom. Similar to learners acquiring knowledge from a teacher and interacting with their peers, TLBO incorporates these interactions [78]. In this study, a value of  $N_p = 100$  is used.

*Generalized oppositional teaching learning based optimization (GOTLBO)*. This method utilizes generalized opposition-based learning to enhance basic TLBO through the initialization step and generation jumping, improving convergence speed [79]. The values of jumping rate  $Jr = 1.0$  and  $N_p = 20$  were used.

*Simplified teaching-learning based optimization algorithm (STLBO)*. In STLBO, the teacher phase is redefined and simplified, while the learner phase remains unchanged [80]. In the redefined teacher phase, the mutation of potential solutions is possible, with the mutation probability decreasing as the iteration number increases. During the early stages, a higher mutation probability helps explore a larger solution space and approach the optimum quickly. However, in the latter stages of optimization, when the teacher (best solution) is near the global optimum, a lower mutation probability serves as a fine-tuning mechanism to enhance local search capability, proving to be an effective strategy. To enrich the mutation behavior, a chaotic sequence is introduced to generate values for the mutation parameters. A chaotic sequence is a deterministic, random-like process found in nonlinear dynamic systems, which is non-periodic, non-converging, and bounded [81]. Additionally, the elite strategy replaces the worst solutions in the current population with new solutions based on objective function values. The logistic chaotic map and  $N_p = 20$  were used.

*Water wave optimization (WW)* takes inspiration from shallow water wave models and incorporates ideas from wave propagation, refraction, and breaking [82]. WW is easy to implement with a small-size population, and there are four control parameters: the maximum wave height  $h_{max}$ , the wavelength reduction coefficient  $\alpha$ , the breaking coefficient  $\beta$ , and the maximum number  $k_{max}$  of breaking directions. According to Zheng [82], we used the values  $h_{max} = 6$ ,  $\alpha = 1.026$ ,  $N_p = 10$ ,  $k_{max} = \min(12, D/2) = 4$ , and  $\beta$  linearly decreased from 0.25 to 0.001.

*Improved JAYA (IJAYA)*. Jaya algorithm is based on the concept that the solution obtained for a given problem should move toward the best solution and should avoid the worst solution and does not require any algorithm-specific parameter [83]. In IJAYA [84], a self-adaptive weight mechanism is introduced to balance the approach towards the optimal solution while simultaneously avoiding the suboptimal solutions. An experience-based learning strategy is utilized to preserve population diversity and enhance exploration capabilities. Additionally, a chaotic elite learning method is proposed to refine the quality of the best solution in each generation. The logistic chaotic map and  $N_p = 4 \times D = 32$  were used.

*Improved sine cosine algorithm (ISCA)*. SCA is based on simulating the behaviors of sine and cosine mathematical functions [85]. ISCA implementation included a modified position-updating equation based on inertia weight ( $w_{start} = 1$ ,  $w_{end} = 1$ ), a nonlinear conversion parameter strategy based on the Gaussian function ( $a_{start} = 2$ ,  $a_{end} = 0$ ) [86], the creation of the opposite population to jump out from the local optima with  $Jr = 0.1$  [87], a greedy selection, and  $N_p = 30$ .

The majority of the algorithms used show excellent performance in estimating the SC parameter within conventional models such as SDM or DDM [76, 67, 79, 84, 74, 73, 80, 78, 88, 16].

In meta-heuristic optimization methods, the quality of the extracted parameters is evaluated using the fitness function at every iteration. In our investigation, we considered absolute error and square error fitness functions:

$$F_{AE}(Y) = \sum_{k=1}^p \left| V^{tr}(I_k) - V^{cal}(I_k, Y) \right|, \quad (8)$$

$$F_{SE}(Y) = \sum_{k=1}^p \left[ V^{tr}(I_k) - V^{cal}(I_k, Y) \right]^2, \quad (9)$$

where  $V^{tr}(I_k)$  is the simulated value of voltage at current  $I_k$ ,  $V^{cal}(I_k, Y)$  represents the voltage, which is calculated using a set of parameters (i.e.  $Y = \{I_{01}, n_1, R_{p1}, I_{02}, n_2, R_{p2}, R_s, I_{ph}\}$ ) estimated with the help of an algorithm and Eqs. (1)–(2); and  $p$  is the total number of voltage steps in the IV characteristic.

We executed each tested algorithm for  $N_{runs} = 51$  independent runs on every simulated IV curve to generate the statistical results. The search ranges were set as follows:

$I_{01}(\text{mA}) \in [10^{-13}, 1]$ ,  $n_1 \in [0.5, 50]$ ,  $R_{p1}(\Omega) \in [10, 10^6]$ ,  $I_{02}(\text{mA}) \in [10^{-7}, 10]$ ,  $n_2 \in [0.5, 50]$ ,  $R_{p2}(\Omega) \in [10, 5 \cdot 10^4]$ ,  $R_s(\Omega) \in [0.1, 1000]$ ,  $I_{ph}(\text{mA}) \in [10^{-3}, 100]$ .

## 2.4. Evaluation metrics

To better illustrate the performance differences between the algorithms being compared, we considered several evaluation metrics. These metrics can be described as follows:

1. Mean value (MEAN), median value (MEDIAN), standard deviance (STD), and interquartile range (IQR) for each two-diode model parameter  $y$  ( $y$  is one of  $\{I_{01}, n_1, R_{p1}, I_{02}, n_2, R_{p2}, R_s, I_{ph}\}$ ). MEAN and MEDIAN are often used to measure the solution quality. The closer the obtained MEAN and MEDIAN values are to the actual parameter values, the closer the obtained solution is to the optimal solution. To quantify, we used the absolute percentage error (APE):

$$\text{APE}(y) = \left| \frac{y - y^{\text{tr}}}{y^{\text{tr}}} \right|, \quad (10)$$

where  $y^{\text{tr}}$  is the parameter value used during the *IV* curve simulation. APE was calculated for  $y_i$ , obtained by one-run algorithm application ( $\text{APE}_i$ ), MEAN ( $\text{APE}_{\text{MEAN}}$ ), and MEDIAN ( $\text{APE}_{\text{MEDIAN}}$ ). Reducing STD and IQR result in a more stable algorithm performance.

2. Another criterion for evaluating and comparing algorithm performance is their execution time. We used average run time  $t_{\text{run}}$  in seconds for an individual optimizer on one *IV* curve.
3. The root mean square percentage error (RMSPE) is a statistical measure that indicates how well the fitted curve matches the actual (simulated) *IV* curve.

$$\text{RMSPE} = \sqrt{\frac{1}{p} \sum_{k=1}^p \left[ \frac{V^{\text{tr}}(I_k) - V^{\text{cal}}(I_k, Y)}{V^{\text{tr}}(I_k)} \right]^2}. \quad (11)$$

4. Wilcoxon signed-rank test is a nonparametric statistical test used for pairwise comparisons of algorithms. This test assigns a rank to all the scores considered as one group and then sums the ranks of each group.
5. Friedman, Friedman Aligned, and Quade tests are used for comparing the performance differences among optimization algorithms (multiple comparisons with a control method). Therefore, the average rankings of the algorithms according to the tests are reported. Besides, the post-hoc Finner, Holm, Hochberg, and Holland procedures are used to establish proper comparisons between each algorithm and a set of other algorithms.
6. Multiple Comparisons Test (Friedman) with Shaffer's static, Nemenyi, and Holm procedures are employed to compute all possible pairwise comparisons between groups ( $N \times N$ ) and identify the differences.

Wilcoxon test is used to assess whether there are statistically significant differences between pairs of algorithms. Meanwhile, the Friedman, Friedman Aligned, and Quade tests are employed when it's necessary to compare three or more related groups of results (algorithms). Friedman test evaluates whether there are statistically significant differences between the medians of the ranks of these algorithms. Friedman Aligned Ranks test addresses the issue of rank correlation in the original Friedman test, providing more precise results. Finally, the Quade test helps account for the effects of observed factors, such as random variations, to more accurately determine the statistical differences between groups.

The main drawback of the Friedman, Friedman Aligned, and Quade tests is that they can only detect significant differences over the whole set of multiple comparisons, making it difficult to establish proper comparisons between specific algorithms [89]. To address these issues, it is necessary to employ post-hoc procedures. Post-hoc methods are applied after the initial analysis and allow for controlling the overall error rate when comparing multiple algorithms, thereby reducing the likelihood of randomly identifying statistically significant differences.

$1 \times N$  designs help determine if there are statistically significant differences between one algorithm (the control algorithm) and each of the other algorithms. Multidimensional comparisons  $N \times N$  designs involve analyzing statistical differences between all possible pairs of algorithms. Typically, different post-hoc procedures are used for  $1 \times N$  and  $N \times N$  comparisons. Description of all the used post-hoc procedures can be found in Derrac *et al.* [89].

All mentioned methods are standard for comparing metaheuristic algorithms [89]. Their comprehensive application enables making the most well-founded conclusions.

**Table 1**

The convergence parameters for metaheuristic algorithms in a single-IV case

Algorithm	$N_{it}$	$N_{FE}$	$t_{run}$ (s)
DE	8000	1024000	42 ± 1
EBLSHADE	3000	444600	22 ± 1
ADELI	12000	1800000	93 ± 2
NDE	5000	430000	20.2 ± 0.3
MABC	8000	1024000	48 ± 11
TLBO	5000	1000000	56.1 ± 0.3
GOTLBO	6000	360000	15 ± 1
STLBO	13000	273000	13.8 ± 0.3
PSO	4000	480000	19 ± 3
IJAVA	30000	960000	37 ± 1
ISCA	5000	150000	6.5 ± 0.1
NNA	5000	250000	10.6 ± 0.5
CWOA	3000	300000	16.6 ± 0.5
WW	3000	35000	1.4 ± 0.1

### 3. Numerical results and discussion

#### 3.1. Comparison of algorithm convergence

In meta-heuristic algorithms, various termination conditions can be defined. For instance, a termination condition can be a specific number of iterations  $N_{it}$ , constraints on the number of fitness function evaluations  $N_{FE}$ , a specific rate of precision, a specific time, no sign of change in solutions after a specific number of iterations, or a combination of these cases [90]. In this study, the main focus was on accurately estimating parameters. Therefore, to ensure that both exploration and exploitation processes could be fully realized by each algorithm with an equal opportunity, the termination criterion used was the absence of changes in the solution. Based on this condition, the required number of iterations  $N_{it}$  was determined, and the corresponding calculation time was measured  $t_{run}$ . Fig. S1 in the supplementary material shows the convergence curve for the algorithms used. In addition, the  $N_{FE}$  were evaluated.

All the applied algorithms have been coded and implemented in Embarcadero®Delphi 10.3 programming software. The run time was estimated by using WinAPI-functions *QueryPerformanceCounter()* and *QueryPerformanceFrequency()*. The experiments were performed on Windows 10 Pro 64-bit, 2.9 GHz AMD Ryzen 7 4800H CPU, and 8 GB RAM.

The obtained results are listed in Table 1. As can be seen from the table, the number of iterations required for an algorithm does not always correlate directly with the number of fitness function evaluations or computation time needed to converge. The reason for this is the unique mathematical operations required by each algorithm. The run time of the algorithms varies considerably, with a range of 1.5 seconds to 93 seconds. Notably, WW, ISCA, NNA, and STLBO converge the fastest, while ADELI, TLBO, and MABC require the most time.

#### 3.2. Fitness function selection

To choose the more suitable fitness function, we evaluated each algorithm using the IV curve generated from the parameters provided in Eq. (3) with both  $F_{AE}$  and  $F_{SE}$  functions (see Eqs. (8) and (9)). The results obtained from each of the functions were then compared with each other using pairwise comparisons. The absolute percentage error values obtained for one-run algorithm application ( $APE_i$ ) were used. Table 2 gives the statistical results produced by Wilcoxon sign-rank test with a significant level  $\alpha = 0.05$ . The symbol “SE” in a cell indicates that the estimation of the parameter (specified in the column title) by the algorithm (defined in the first column) with  $F_{SE}$  outperforms the result obtained by this algorithm with  $F_{AE}$ . A cell with “AE” indicates better results for function  $F_{AE}$ . In the case of the symbol “=”, there is no significant difference between function  $F_{SE}$  and function  $F_{AE}$  application.

As evidenced in the provided data, utilizing the square error fitness function more frequently yields better outcomes than  $F_{AE}$ . In some rare cases, the absolute error fitness function can improve the alignment between the fitted and actual curves and enhance the accuracy of parameter estimations by PSO, IJAVA, CWOA, and WW algorithms. However, RMSPE is not the most crucial factor in determining model parameters, and the mentioned methods, as will be shown

**Table 2**Wilcoxon signed rank test results (level of significance  $\alpha = 0.05$ ) for comparing fitness functions.

Algorithm	Parameter								
	$I_{01}$	$n_1$	$R_{p1}$	$I_{02}$	$n_2$	$R_{p2}$	$R_s$	$I_{ph}$	RMSPE
DE	SE	SE	=	=	SE	SE	=	=	=
EBLSHADE	SE	=	=	=	=	=	=	=	AE
ADELI	SE	=	=	=	=	=	=	=	AE
NDE	=	=	=	=	=	=	=	SE	SE
MABC	=	SE	=	=	=	=	=	=	SE
TLBO	SE	SE	SE	SE	SE	SE	SE	SE	SE
GOTLBO	=	=	=	=	=	SE	=	=	=
STLBO	SE	=	=	=	=	=	=	=	AE
PSO	=	=	=	=	=	=	AE	=	=
IJAYA	AE	AE	=	=	SE	=	=	=	=
ISCA	=	=	=	=	=	=	=	=	=
NNA	=	=	=	=	=	=	=	=	SE
CWOA	=	=	SE	=	AE	=	=	=	SE
WW	=	=	SE	=	AE	=	=	=	SE

later, do not provide the highest accuracy. As such, the results presented in the following sections exclusively apply the  $F_{SE}$  function. Therefore, it is recommended that researchers consider the squared error fitness function as a more effective and reliable option for the task of opposed two-diode model parameter estimation.

### 3.3. Comparison of algorithm performance

#### 3.3.1. Parameter extraction in single-IV case

In this subsection, we present and analyze the statistical results of applying different meta-heuristic algorithms to an IV curve simulated with the values from Eq. (3). Several typical fitting results are shown in Fig. 2. A more comprehensive version, including the fitting results obtained using each algorithm, is provided in the supplementary materials (figure S2). It can be seen that the closest match between the approximation curves and the IV curve points is observed for EBLSHADE, ADELI, NDE, IJAYA, TLBO, and STLBO. On the contrary, the fitting curves of PSO and GOTLBO had the least replication of the original data.

Fig. 4 shows the results of SC parameters estimation by algorithms to be compared. Additionally, the figure presents the RMSPE data, which confirms the conclusions of the visual comparison between the fitting lines and the points of the IV curve. The results for MEAN, MEDIAN, STD, and IQR are presented in table S1 of the supplementary material.

We want to emphasize the following. Firstly, in most cases, median values are more relevant to the actual parameter values than mean values. The only exceptions to this are in the estimation of  $R_s$  and  $R_{p2}$ . However, in cases where a method allows for highly accurate parameter estimation (such as EBLSHADE, ADELI, TLBO, and STLBO), the MEDIANs are at least as good as the MEANS. As a result, we will utilize median values as a robust measure of central tendency in nonparametric statistical tests. Secondly, the increased algorithm stability, as indicated by the reduction in STD and IQR values when determining each model parameter, correlates with improved accuracy in estimating those parameters. Furthermore, IQR values are generally no worse than STD values. Finally, small RMSPE values (a close match between the fitting curve and the IV points) do not always indicate high accuracy in determining the parameters of a solar cell — see IJAYA and NDE data. For example, the difference between the MEDIAN<sub>RMSPE</sub> values for NDE and ADELI is approximately 0.0001 (about 0.08% of their absolute value). However, in the ADELI case, the values of APE<sub>MEDIAN</sub> do not exceed  $6 \cdot 10^{-4}$  for all model parameter estimations. In contrast, when applying the NDE algorithm, the obtained APE<sub>MEDIAN</sub> values are significantly higher, ranging from 0.04 for  $I_{ph}$  to 11.4 for  $I_{01}$ . On the one hand, this confirms the previously mentioned issue identified by Tada [46, 53], which arises when estimating parameters according to the opposed two-diode model from similar IV curves corresponding to PV cells with distinct characteristics. Furthermore, the results indicate that some meta-heuristic algorithms, such as NDE and IJAYA, can fall into a similar trap. On the other hand, the high accuracy in parameter estimation demonstrated by EBLSHADE, ADELI, and STLBO indicates that these algorithms can overcome the mentioned issue when applied. It should be noted that a similar problem has been previously addressed using Bayesian parameter estimation [53]. However, each

## Meta-heuristic parameter extraction of SCs with S-shaped IV curves

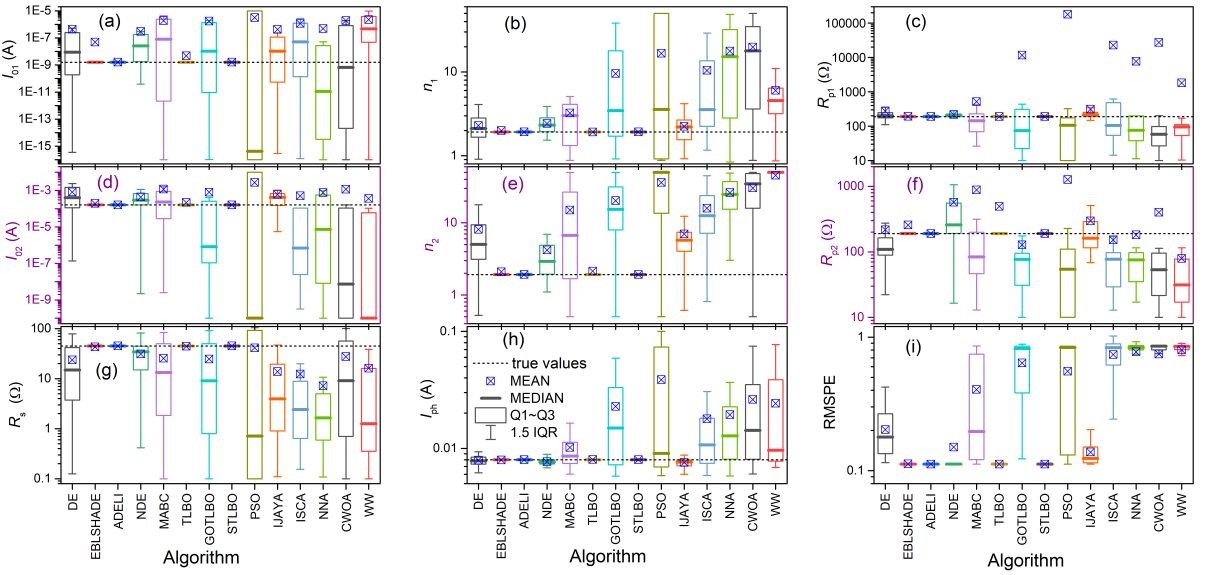


**Figure 4:** Box-plot of parameter estimation results by using different optimization algorithms. The single-IV case. The squares represent the mean values, and the dashed lines correspond to the true parameter values.

Bayesian calculation took approximately half a day on a more powerful computer than ours [53]. In contrast, when applying meta-heuristic algorithms in our case, the worst-case run time did not exceed 100 seconds.

To statistically compare the algorithms under consideration, we used nonparametric tests. In the single-IV case, all nonparametric statistical tests were applied to compare the performance of meta-heuristic algorithms in assessing each of the eight model parameters.  $APE_i$  values were used, and the number of case problems in the study,  $N_{pr}$ , was equal to  $N_{runs} = 51$ . Additionally, algorithms were compared in terms of curve-fitting accuracy using RMSPE values. Furthermore, we employed tests for a composite parameter as well. This parameter, referred to as “Comp” hereafter, includes  $APE_{MEDIAN}$  for each of the eight defined model parameters, the median value for RMSPE, and  $t_{run}$ . This composite parameter may provide the most valuable insights for comparing the performance of the algorithms. However, it is important to note that the value of  $N_{pr}$  is only 10. According to Derrac *et al.* [89], the number of case problems should be  $N_{pr} \geq 2k$ , where  $k$  is the number of algorithms ( $k = 14$  in our study). Therefore, the use of the Comp parameter is not strictly rigorous. Indeed, it would have been possible to increase the  $N_{pr}$  value by using, for example,  $APE_{MEAN}$ . However, deliberately using a suboptimal parameter would have seemed inappropriate.

Fig. 5 graphically depicts the non-parametric statistical results of pairwise comparisons of the algorithms based on the Wilcoxon signed-rank test. For the Comp parameter comparisons, the differences in the performance scores were normalized to the interval  $[0, 1]$  to facilitate the comparison. The figure shows that no single algorithm outperforms all the others in evaluating each parameter. Furthermore, no algorithm surpasses all the others when estimating even a single parameter.

For example, as the figure states, STLBO shows a significant improvement over DE, NDE, MABC, GOTLBO, PSO, IJAYA, ISCA, NNA, CWOA, and WW across all the parameters considered with a level of significance  $\alpha = 0.05$ . Simultaneously, no significant differences were detected between the STLBO algorithm and both the EBL SHADE and ADEL I algorithms for the estimation of all parameters. Additionally, no significant differences were found between STLBO and TLBO for the Comp parameter comparisons. EBL SHADE outperforms almost all other algorithms in the composite parameter except STLBO. According to the count of victories in the Wilcoxon test, the worst performances are exhibited by PSO and CWOA. PSO achieved better results than ISCA, NNA, and CWOA in RMSPE value and also outperformed WW in  $n_2$  estimation and RMSPE. Test detected significant differences between CWOA and WW in  $n_2$  and  $I_{01}$  estimations, between CWOA and PSO in  $I_{01}$ ,  $I_{02}$ ,  $R_s$ , and  $I_{ph}$  estimations, and between CWOA and both ISCA and NNA in  $R_s$  estimation only.

Looking at the results of the Wilcoxon test from another perspective, it can be observed that neither EBL SHADE nor STLBO suffered any defeats in pairwise comparisons, while ADEL I experienced only one loss. ADEL I was defeated in the Comp parameter only by EBL SHADE, primarily due to significantly longer run time. The highest

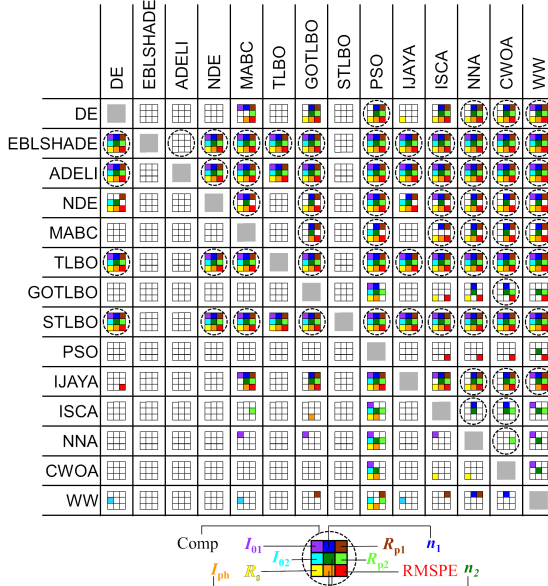


**Figure 5:** The results of Wilcoxon signed-rank test with a level of significance  $\alpha = 0.05$  in the single-IV case. Each colored small square indicates that the algorithm specified in the row outperforms the algorithm specified in the column in evaluating one of the parameters of the two-diode model. The correspondence between the color and position of the square to a model parameter is shown in a legend at the figure bottom. The advantage of the row algorithm in the Comp parameter is indicated by the presence of a dashed circle.

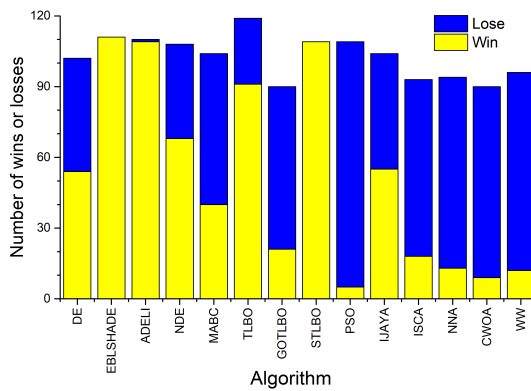


**Figure 6:** The total count of wins and losses for each algorithm in pairwise comparisons using the Wilcoxon signed-rank test with a significance level of  $\alpha = 0.05$  in the single-IV case.

number of defeats was observed for the PSO and WW algorithms (104 and 84, respectively). Fig. 6 summarizes the total number of wins and losses in the Wilcoxon test for each algorithm.

It is recommended [89] to initiate the multiple comparison tests by examining the null hypothesis  $H_0$ , which asserts the equality of medians among the populations of results obtained by different algorithms. The  $p$ -values for the null hypothesis, computed through the statistics of Friedman, Friedman Aligned, and Quade tests and the Iman–Davenport extension, are provided in the supplementary material (table S2). The highest observed  $p(H_0)$ -values were found to be  $2.7 \cdot 10^{-5}$  (Friedman Aligned test for the task of  $R_p$  estimation),  $4.4 \cdot 10^{-4}$  (Friedman Aligned test for the composite parameter case), and  $8.3 \cdot 10^{-6}$  (Quade test, Comp parameter). Thus, the obtained data strongly suggest the significant differences among the considered algorithms in the accuracy of all model parameter determination, RMSPE values, and the Comp parameter.

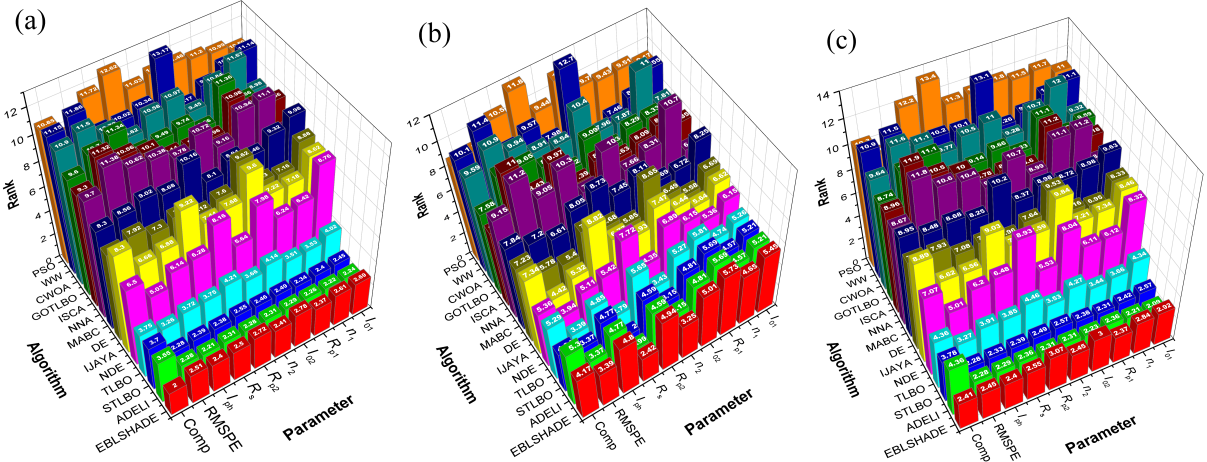


**Figure 7:** Ranking of the algorithms according to Friedman (a), Friedman Aligned (b), and Quade (c) tests in the single-IV case.

Fig. 7 illustrates the ranks achieved by the Friedman, Friedman Aligned, and Quade tests for the applied optimization algorithms in different tasks. These ranks are also tabulated in the supplementary material (table S3). In nearly all cases, the algorithms EBL SHADE, ADELI, and STLBO consistently achieve the top three ranks. For instance, in assessing the accuracy of model parameter estimation, ADELI has ranked first 22 times. The STLBO algorithm ranked first six times, taking the sole first place twice ( $I_{01}$  estimation according to Friedman Aligned test and  $R_{p1}$  estimation according to Quade test) and sharing it with ADELI four times ( $n_1$ ,  $R_{p1}$ ,  $n_2$ , and  $I_{ph}$  estimation according to Friedman Aligned test). In the RMSPE case, ADELI and STLBO attained equal and top ranks across all three tests utilized. When comparing based on the Comp parameter, the STLBO algorithm secured the top rank according to the Friedman Aligned test, whereas the Friedman and Quade tests identified EBL SHADE as the best performer. For the most part, the TLBO algorithm consistently ranked fourth among all the tested algorithms. Interestingly, in four cases ( $I_{01}$  estimation, RMSPE value, and Comp parameter by Friedman Aligned test, and Comp parameter by Quade test), it even achieved a commendable third-place ranking. We must note that overall, the absolute values of ranks for the ADELI, STLBO, EBL SHADE, and TLBO algorithms differ only slightly, and the difference between the first and fourth ranks is often less than 0.5. The worst ranks are observed for PSO, NNA, CWOA, and WW.

It is known [89] that the Friedman, Friedman Aligned, and Quade tests are inadequate for establishing accurate comparisons between the considered algorithms. To compare a control method (one of 14 tested) with a set of other algorithms (the remaining 13), one can define a family of null hypotheses related to the control method. Applying a post-hoc procedure makes it possible to obtain a  $p$ -value that indicates the probability of obtaining the observed results if the corresponding hypothesis is true. We calculated  $p$ -values using four post-hoc procedures (Finner, Holm, Hochberg, and Holland) for all algorithms, tests, and tasks. The reader is referred to the supplementary material for all  $p$ -values (Tables S4-S143). In particular, a common feature of all comparisons is that the Finner post-hoc procedure demonstrates the most powerful behavior, yielding the lowest  $p$ -values.

In our study, we adopted a threshold value of  $p_{cr} = 0.1$  to establish a critical level for comparing the algorithms' effectiveness in both multiple  $1 \times N$  and  $N \times N$  comparisons. That is, it was defined that the likelihood of obtaining a result as extreme as the observed one if there is no difference between the two algorithms (null hypothesis), was less than 10%.

The statistical results of the comparison of algorithm effectiveness are available in the supplementary materials (figure S3). Among the compared algorithms, EBL SHADE, ADELI, and STLBO consistently outperform the others in  $1 \times N$  multiple comparisons. On the other hand, algorithms such as PSO, ISCA, CWOA, and NNA consistently yield lower-quality results. The main changes observed in nonparametric statistical estimation of different parameters evaluation mainly concern algorithms with moderate effectiveness.

In all cases, the Quade test yields higher adjusted  $p$ -values. In particular, in the case of the complex parameter, the  $p$ -value for any comparison did not exceed the chosen threshold value  $p_{cr}$ .

**Table 3**

The total count of wins and losses for each algorithm in  $1 \times N$  multiple comparisons using the Friedman, Friedman Aligned, and Quade tests and Finner, Holm, Hochberg, and Holland post-hoc procedures in single-IV case. The criterion for victory was a adjusted  $p$ -value less than 0.1.

Algorithm	Wins / Loses									Total	
	task										
	$I_{01}$	$n_1$	$R_{p1}$	$I_{02}$	$n_2$	$R_{p2}$	$R_s$	$I_{ph}$	RMSPE	Comp	
DE	24/43	56/34	48/35	4/73	48/43	49/34	49/40	45/35	49/48	16/27	388/412
EBLSHADE	<b>108/0</b>	<b>108/0</b>	<b>107/0</b>	<b>103/0</b>	<b>107/0</b>	<b>104/0</b>	111/2	<b>105/0</b>	<b>109/0</b>	<b>88/0</b>	1050/2
ADELI	<b>122/0</b>	<b>110/0</b>	<b>107/0</b>	<b>128/0</b>	<b>110/0</b>	<b>122/0</b>	<b>119/0</b>	<b>105/0</b>	<b>109/0</b>	61/2	<b>1093/2</b>
NDE	35/19	56/32	56/19	36/49	77/32	23/45	73/32	48/8	83/29	23/20	519/285
MABC	8/61	28/69	44/45	9/57	40/55	4/82	32/51	32/66	44/62	8/30	249/578
TLBO	80/3	<b>102/0</b>	<b>101/0</b>	84/13	<b>99/0</b>	87/18	93/10	<b>94/0</b>	<b>100/0</b>	65/2	905/46
GOTLBO	8/60	12/73	4/84	16/49	20/74	13/54	20/61	4/80	16/85	13/28	126/648
STLBO	<b>109/0</b>	<b>110/0</b>	<b>107/0</b>	<b>125/0</b>	<b>107/0</b>	<b>119/0</b>	<b>116/0</b>	<b>105/0</b>	<b>109/0</b>	<b>81/0</b>	1088/0
PSO	0/84	8/88	0/100	0/108	4/101	0/96	0/124	0/96	20/70	4/49	72/916
IJAYA	28/28	56/34	48/35	13/52	45/43	54/34	20/61	56/29	57/38	16/34	393/388
ISCA	8/56	12/76	4/84	12/45	28/65	16/51	8/61	17/68	0/92	16/32	121/630
NNA	33/29	0/92	4/84	12/49	12/84	12/57	8/77	12/80	0/92	0/52	93/696
CWOA	8/60	0/96	4/80	8/52	8/84	4/83	20/61	0/88	0/92	0/52	52/748
WW	0/96	12/76	16/76	36/43	0/108	10/60	12/77	12/66	0/92	0/52	98/844

The adjusted  $p$ -values obtained from the direct comparisons of EBL SHADE, ADELI, and STLBO do not allow for determining the best algorithm among them. However, for this purpose, the results of this top trio of algorithms can be used, obtained from their comparisons with less efficient optimization methods. Table 3 summarizes count of wins and losses for each algorithm in  $1 \times N$  multiple comparisons. The maximum possible number of wins achieved in every 10 tasks is 156, obtained from comparing with 13 algorithms in 3 tests using 4 procedures. As can be seen, among the compared algorithms, ADELI showed the highest count of statistically confirmed improvements (1093) over others, indicating its superior performance. Conversely, STLBO demonstrated the lowest count of defeats (0) in similar comparisons, suggesting its consistently strong performance.

Previously, we employed procedures that controlled the Family-Wise Error Rate (FWER) for comparisons with a control algorithm. We tested each of the 14 algorithms individually to determine if any of them were superior to the others. Below are the results of the carried out a multiple comparisons in which all possible pairwise comparisons need to be computed ( $N \times N$  comparison), and three procedures (Shaffer's static, Nemenyi, and Holm) have been used to control FWER. These procedures take into account that the hypotheses being tested belonging to a family of all pairwise comparisons are logically interrelated; thus not all combinations of true and false hypotheses are possible.

Starting from the analysis performed by the Friedman test over our results, we can raise the 91 hypotheses of equality among the 14 algorithms of our study for each task, and apply the methods mentioned earlier to contrast them. Table 4 lists the part of the hypotheses and the adjusted  $p$ -values achieved on the task of  $I_{01}$  estimation. For the remaining 46 hypotheses not indicated in the table, a  $p$ -value of 1 was obtained after applying each of the procedures. The full version of the table as well as the data, obtained for other task, are given in the supplementary material (tables S144-S153).

It can be seen that using a level of significance 0.1, only 37 hypotheses of equality are rejected by the Nemenyi, Holm, and Shaffer methods. These hypotheses show the improvement of EBL SHADE, ADELI, TLBO, and STLBO over DE, NDE, MABC, GOTLBO, PSO, ISCA, NNA, CWOA, and WW, and NNA over WW. None of the remaining 54 hypotheses can be rejected using these procedures.

It should be noted that when testing complementary hypotheses ("algorithm A vs algorithm B" and "algorithm B vs algorithm A"), only in one out of the two cases can a  $p$ -value less than 1 be obtained. For instance, when using the Nemenyi procedure to task  $I_{01}$  evaluating of comparing "ADELI vs MABC" a  $p$ -value of  $5.84 \cdot 10^{-9}$  was obtained. Conversely, when comparing "MABC vs ADELI", the  $p$ -value was 1. The  $p$ -values were computed for all possible hypotheses in the study to identify algorithms whose results statistically deviate from those of other algorithms. In this case, a critical value of  $p_{cr} = 0.1$  was used, similar to the  $1 \times N$  multiple comparisons. Typical examples of the

obtained results for specific parameter cases are presented in Fig. 8. For more comprehensive data, please refer to figure S3 in the supplementary materials. Generalized results regarding the total count of victories and defeats in the  $N \times N$  comparisons are listed in Table 5. In the case of  $N \times N$  comparisons, the maximum possible number of wins achieved in every 10 tasks is 39, obtained from comparing 13 algorithms in 3 post-hoc procedures.

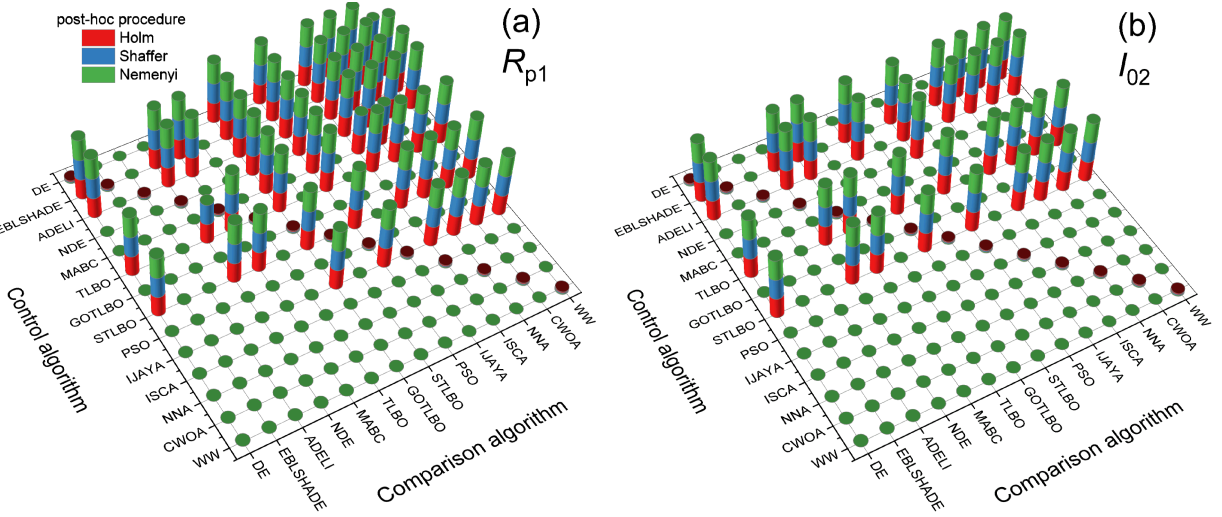


**Figure 8:** The results of  $N \times N$  multiple comparisons of  $R_{p1}$  (a) and  $I_{02}$  (b) estimation among all algorithms in the single-IV case. The colored cylinder indicates that the adjusted  $p$ -value, which tests the control algorithm outperforms the comparison algorithm, is not greater than  $p_{lim} = 0.1$ . The correspondence between the color of the cylinder to a post-hoc procedure is shown in the figure's legend.

In the majority of cases, all post-hoc procedures considered lead to similar conclusions regarding the outperforming of one algorithm over another. For example, in the case of the  $R_{p1}$  estimation task, the Nemenyi procedure disagrees with Holm and Shaffer methods in only 4 out of 57 cases. Specifically, this occurs for the hypotheses "DE vs WW," "MABC vs ISCA," "MABC vs NNA," and "TLBO vs NDE" — see Fig. 8(a). On the other hand, as evident from Fig. 8(b), such situations are not observed at all for the  $I_{02}$  task. The Holm procedure results, in general, differs from the Shaffer procedure ones in only two comparisons: the improvement of IJAYA over GOTLBO in the  $n_1$  estimation and the outperforming of TLBO over NNA for the composite parameter.

Totally  $1 \times N$  multiple comparisons exhibit more powerful behavior than  $N \times N$  ones, reaching the lower  $p$ -values. As a result, IJAYA did not lose in any of the  $N \times N$  comparisons — see Table 5. Another striking example can be observed when considering the case of the composite parameter. Based on the  $1 \times N$  comparisons, conclusions were drawn about the outperforming of one algorithm over another in 67 cases, whereas for the  $N \times N$  comparisons, such situations were found in only 20 cases: the improvement of EBLSHADE over MABC, GOTLBO, PSO, ISCA, NNA, CWOA, and WW, the statistically significant difference ADELI and GOTLBO, PSO, NNA, CWOA, and WW, and outperforming of both TLBO and STLBO over PSO, NNA, CWOA, and WW. Consequently,  $N \times N$  comparisons provide a less precise ranking of all algorithms. However, it is still possible to identify the best and worst-performing algorithms. The obtained data reveal that EBLSHADE, ADELI, and STLBO are the top-performing algorithms in all tasks, while PSO, ISCA, NNA, CWOA, and WW are the worst-performing.

Thus, the results presented in this subsection demonstrate that among the examined algorithms, none can be applied for the maximally accurate determination of a specific individual parameter (e.g., only  $R_{p2}$  or only  $I_{ph}$ ) in the opposed two-diode model. The algorithms that exhibit high efficiency (EBLSHADE, ADELI, and STLBO) allow for the most precise estimation of all parameters. However, certain algorithms really display higher accuracy in determining specific parameters. Indeed, DE and IJAYA are the most effective in estimating  $R_{p2}$  and  $I_{ph}$  — see table S1. Nevertheless, this highest level of accuracy appears unworthy of significant attention when compared to other optimization methods. As a result, the performance metrics of algorithms for individual parameters will not be analyzed in the following subsection, dedicated to the analysis of IV curves with different parameter ratios.

### 3.3.2. Parameter extraction in IV-set case

Fig. 3 shows several typical fitting results of a set of synthetic IV curves simulated according to the opposed two-diode model using the parameter values described in Sec. 2.2.2. A more comprehensive and enhanced version, including the fitting results obtained using each algorithm, is provided in the supplementary materials (figure S4). Similar to the single-IV case, the algorithms EBL SHADE, ADELI, NDE, IJAYA, TLBO, and STLBO show the highest agreement between the fitting curves and the points of synthesized current-voltage curves. Fig. 9 represents a portion of the results obtained from evaluating solar cell parameters using various algorithms, along with the corresponding RMSPE data. The supplementary material provides the dependencies of all parameters on synthesis temperature as determined by all the algorithms — see figures S5-S13. The results in terms of MEAN, MEDIAN, STD, and IQR are tabulated as well (table S154 in the supplementary material).

It should be noted that in several cases, the accuracy of parameter estimation depends on temperature, even for constant parameters. For instance, as the temperature increases, the errors in determining  $R_{p1}$  by NDE, MABC, GOTLBO, IJAYA, ISCA, and WW decrease. However, under the same conditions, the estimation quality of  $I_{01}$  using DE, ISCA, and WW worsens. These results indicate that the accuracy of parameter estimation depends not only on the parameter value itself but also on its ratio with other parameters. A comprehensive investigation into the specific dependencies of parameter estimation accuracy for each algorithm has not been conducted. This study aimed to determine the best algorithms rather than elucidate the peculiarities of their application in the context of opposed the two-diode model.

The presented data display several characteristics that were also observed in the single-IV case. For instance, the error in parameters estimating by mean values is higher compared to that of median values in the majority of cases. Exceptions are observed at some temperatures only when evaluating  $I_{01}$  using IJAYA,  $n_1$  using IJAYA and DE,  $R_{p1}$  using DE and MABC, and  $R_s$  using DE and WW. However, for high-precision algorithms, the deviation of MEDIAN from the true value does not exceed the deviation of MEAN. Additionally, these algorithms exhibit small IQR values that do not exceed STD. Similar to the previous case, small RMSPE values do not always indicate high accuracy in determining the parameters of a solar cell.

At the same time, the number of algorithms exhibiting minimal errors has decreased. Significant deviations from true values are observed for median values of  $I_{01}$ ,  $n_1$ ,  $R_{p1}$ ,  $n_2$ ,  $R_s$ , and  $I_{ph}$  evaluated by EBL SHADE at various temperatures, as well as for median values of diode D1 characteristics and series resistor determined using TLBO at 260 K. Thus, only ADELI and STLBO remain as algorithms without visible errors. Although this claim of infallibility applies only to median values, substantial errors are observed for mean values in several cases. Simultaneously, EBL SHADE, TLBO, IJAYA, and NDE form a group of algorithms with low RMSPE values but imperfect model parameter estimation.

In the IV-set case, to assess the statistical performance of compared algorithms, the run time and all  $\text{APE}_{\text{MEDIAN}}$  and  $\text{RMSPE}_{\text{MEDIAN}}$  for each IV curve were taken into account. This approach is similar to the use of the Comp parameter in the previous subsection; however, in this scenario,  $N_{pr} = 81$  is employed:

$$N_{pr} = 10 T_{\text{values}} \times (8 \text{APE}_{\text{MEDIAN}} + 1 \text{RMSPE}_{\text{MEDIAN}}) + 1 t_{\text{run}}.$$

Therefore, such an approach is well-suited for nonparametric statistical analysis of  $k = 14$  meta-heuristic algorithms. Certainly, at first sight, it would be interesting to consider incorporating an additional 80 values of the interquartile range into the dataset. This approach could provide consideration into the stability of algorithm performance as well. However, it is known [89] that for multiple comparisons, a value of  $N_{pr} \geq 8 \cdot k = 112$  could be too high, obtaining no significant comparisons as a result.

Table 6 gives the statistical results produced by the Wilcoxon sign–rank test. As the table states, ADELI outperforms all other algorithms with a level of significance  $\alpha = 0.05$ . STLBO and TLBO show an improvement over DE, EBL SHADE, NDE, MABC, GOTLBO, PSO, IJAYA, ISCA, NNA, CWOA, and WW. The counts of statistical significant cases (+/-) are presented in the last row of Table 6. It can be seen than PSO, ISCA, NNA, and CWOA did not outperform any of the algorithms, whereas WW statistically significantly improved over NNA only. Therefore, although these algorithms have promising run times, they are not recommended for parameter estimation of a solar cell based on the opposed two-diode model.

The  $p$ -values required to test the null hypothesis, computed using the Friedman, Friedman Aligned, Quade tests, and the Iman–Davenport extension, can be found in table S2 of the supplementary materials. None of these values exceeds  $2.3 \cdot 10^{-6}$ , thereby rejecting the hypothesis of equivalent medians in all tests.

Ranks achieved by the Friedman, Friedman Aligned, and Quade tests are shown in Fig. 10 and table S3 in the supplementary material. As per the given results, ADELI has been placed at first rank by Friedman and Quade tests, and STLBO has ranked first by the Friedman Aligned test. TLBO has been recorded as the second-best algorithm by all three tests. Furthermore, PSO was recognized as the worst-performing algorithm by the tests' unanimous decision.

The  $p$ -values, obtained for  $1 \times N$  multiple comparisons are shown in tables S155-168 in the supplementary material. There are results of applying Finner, Holm, Hochberg, and Holland procedures, as a post-hoc method after Friedman, Friedman Aligned, and Quade tests. The reader is referred to supplementary material (table S169) for  $p$ -values of applying Shaffer, Nemenyi, and Holm post-hoc procedures after the Friedman test in the case of  $N \times N$  multiple comparisons. The results, which determine whether one algorithm yielded a statistically better estimation of parameters than the other (with a  $p$ -value  $\leq p_{cr} = 0.1$ ), are summarized in Fig. 11 and 12 for  $1 \times N$  and  $N \times N$  comparisons, respectively. The counts of statistically significant cases are presented in the Table 7.

As can be seen, ADELI, TLBO, and STLBO were never outperformed by any of the algorithms, both in the case of  $1 \times N$  and  $N \times N$  multiple comparisons. By the way, for  $N \times N$  comparisons, the same property is observed with EBL SHADE and IJAYA. Overall, the parameter estimation results obtained from the set of IV curves using ADELI, TLBO, and STLBO algorithms for  $N \times N$  comparisons in the opposed two-diode model are practically indistinguishable (when it comes to precise  $p$ -values, only minor differences can be observed). In  $1 \times N$  comparisons, TLBO demonstrates lower performance compared to ADELI and STLBO, in terms of efficiency when compared to the EBL SHADE algorithm. Specifically, the improvement of TLBO over EBL SHADE is proved only by the Finner procedure applied in the Friedman test. Based on  $1 \times N$  comparisons, it is observed as well that there are slight differences between ADELI and STLBO, primarily when compared to the non-worst algorithms. For instance, the Quade test confirms the improvement of ADELI over EBL SHADE for every post-hoc procedure, however, the Friedman and Friedman Aligned tests did not show statistically significant differences between these algorithms. Meanwhile, the Friedman Aligned and Quade tests find a difference between STLBO and EBL SHADE for every post-hoc procedure and Finner procedure only, respectively. Regarding comparison with NDE, the Friedman Aligned test demonstrated that STLBO is better according to all post-hoc procedures. In contrast, for ADELI, this outperforming was only observed using the Finner method. In the case of IJAYA, the results of the Friedman Aligned test show a reversal: only the Finner procedure indicates an improvement for STLBO, whereas ADELI outperforms all post-hoc methods utilized.

In deciding the optimal algorithm for parameter estimation of solar cell parameters from the IV curve using the opposed two-diode model, the practical choices boil down to EBL SHADE, ADELI, TLBO, and STLBO. However, TLBO exhibited lower performance when applied in the single-IV case. The parameter estimation error when using EBL SHADE was not always minimal in the IV-set case. Despite the minimal advantage in terms of win counts in  $1 \times N$  comparisons (see Table 7), we hesitate to declare STLBO as the best. In our opinion, STLBO and ADELI both hold the top position in the competition conducted in this study.

Over the last few decades, researchers have strived to enhance the performance of metaheuristic algorithms using various concepts, including [17]: hybridization between two or more metaheuristics, quantum computing concept, opposition-based theory, chaotic maps, Lévy-Flight strategy. Our research has revealed that the most promising approaches to solving the parameter estimation problem for S-shaped IV curves involve the use of enhanced mutation strategies. Specifically, this entails employing chaotic maps to tune mutation coefficients and utilizing the elite strategy (STLBO). Furthermore, highly productive results were achieved through the application of nonlinear (polynomial) approximation of potential solutions (ADELI).

## 4. Conclusion

In this paper, the possibility of using meta-heuristic algorithms to solve the parameter estimation problems of photovoltaic cells with S-shaped current–voltage characteristics has been explored. The parameter estimation has been performed within the framework of the opposed two-diode model. A total of 14 meta-heuristic algorithms from various classes were implemented to extract the solar cell parameters from synthetic IV curves, which were generated with a range of parameter values. The obtained results have been compared using nonparametric statistical procedures, including pairwise comparisons,  $1 \times N$  multiple comparisons, and  $N \times N$  multiple comparisons.

Research has demonstrated that utilizing a squared error-based fitness function offers clear advantages in tackling a provided problem. The overall performance results of various algorithms generally fit the No Free Lunch theory. GOTLBO, PSO, ISCA, NNA, CWOA, and WW are completely unsuitable for parameter estimation according to the

opposed two-diode model. The results of DE, NDE, MABC, and IJAYA are not as poor as those in the previous group; however, in general, it is still not recommended to use these algorithms for solving parameter identification problems. Generally, the EBL SHADE and TLBO are effective in accurately determining parameter values in most cases. However, investigation has shown that these algorithms may make mistakes under certain conditions. Therefore, EBL SHADE and TLBO applications in the case of solar cells with S-shaped IV curves should be approached with caution. Finally, results have illustrated that STLBO and ADELI have superior performance in terms of accuracy and reliability when compared with other used algorithms. In particular, these two algorithms successfully solve the task of accurately determining parameters from similar IV curves corresponding to photovoltaic cells with distinct characteristics.

It is important to note that in this study, the parameters were obtained from idealized IV curves, where the voltage-current relationships were precisely defined by Eq. (1). In a real experiment, there is a potential for errors in the measurement of both current and voltage. Hence, it would be worthwhile to explore the efficacy of various meta-heuristic algorithms in determining parameters from IV data corrupted by noise in future research.

This work of testing and comparative analysis of different meta-heuristic algorithms for the estimation of solar cell parameters should be useful for further research and development on photovoltaic systems.

## Supplementary data

Supplementary data to this article can be found online at <http://surl.li/phuem>

## Data availability

Data will be made available on request.

## References

- [1] M. Zhang, W. Zhang, F. Zhang, C.-S. Lee, Y. Tang, Anion-hosting cathodes for current and late-stage dual-ion batteries, *Science China Chemistry* 67 (2024) 1485–1509.
- [2] M. Wang, C. Jiang, S. Zhang, X. Song, Y. Tang, H.-M. Cheng, Reversible calcium alloying enables a practical room-temperature rechargeable calcium-ion battery with a high discharge voltage, *Nat. Chem.* 10 (2018) 667–672.
- [3] X. Zhang, Y. Tang, F. Zhang, C.-S. Lee, A novel aluminum-graphite dual-ion battery, *Adv. Energy Mater.* 6 (2016) 1502588.
- [4] X. Wang, X. Tian, X. Chen, L. Ren, C. Geng, A review of end-of-life crystalline silicon solar photovoltaic panel recycling technology, *Sol. Energ. Mat. Sol.* 248 (2022) 111976.
- [5] D. H. Muhsen, A. B. Ghazali, T. Khatib, I. A. Abed, A comparative study of evolutionary algorithms and adapting control parameters for estimating the parameters of a single-diode photovoltaic module's model, *Renew. Energ.* 96 (2016) 377–389.
- [6] R. Abbassi, A. Abbassi, A. A. Heidari, S. Mirjalili, An efficient salp swarm-inspired algorithm for parameters identification of photovoltaic cell models, *Energy Convers. Manage.* 179 (2019) 362–372.
- [7] T. Sudhakar Babu, J. Prasanth Ram, K. Sangeetha, A. Laudani, N. Rajasekar, Parameter extraction of two diode solar PV model using fireworks algorithm, *Sol. Energy* 140 (2016) 265–276.
- [8] H. M. Ridha, H. Hizam, C. Gomes, A. A. Heidari, H. Chen, M. Ahmadipour, D. H. Muhsen, M. Alghrairi, Parameters extraction of three diode photovoltaic models using boosted LSHADE algorithm and Newton Raphson method, *Energy* 224 (2021) 120136.
- [9] A. Rezaee Jordehi, Enhanced leader particle swarm optimisation (ELPSO): An efficient algorithm for parameter estimation of photovoltaic (PV) cells and modules, *Sol. Energy* 159 (2018) 78–87.
- [10] N. Barth, R. Jovanovic, S. Ahzi, M. A. Khaleel, Pv panel single and double diode models: Optimization of the parameters and temperature dependence, *Sol. Energ. Mat. Sol.* 148 (2016) 87–98.
- [11] J. P. Ram, T. S. Babu, T. Dragicevic, N. Rajasekar, A new hybrid bee pollinator flower pollination algorithm for solar pv parameter estimation, *Energy Convers. Manage.* 135 (2017) 463–476.
- [12] H. M. Ridha, Parameters extraction of single and double diodes photovoltaic models using Marine Predators Algorithm and Lambert W function, *Sol. Energy* 209 (2020) 674–693.
- [13] M. Abdel-Basset, D. El-Shahat, R. K. Chakrabortty, M. Ryan, Parameter estimation of photovoltaic models using an improved marine predators algorithm, *Energy Convers. Manage.* 227 (2021) 113491.
- [14] H. Chen, S. Jiao, A. A. Heidari, M. Wang, X. Chen, X. Zhao, An opposition-based sine cosine approach with local search for parameter estimation of photovoltaic models, *Energy Convers. Manage.* 195 (2019) 927–942.
- [15] A. M. Beigi, A. Maroosi, Parameter identification for solar cells and module using a Hybrid Firefly and Pattern Search Algorithms, *Sol. Energy* 171 (2018) 435–446.
- [16] G. Xiong, J. Zhang, D. Shi, Y. He, Parameter extraction of solar photovoltaic models using an improved whale optimization algorithm, *Energy Convers. Manage.* 174 (2018) 388–405.
- [17] M. Abdel-Basset, R. Mohamed, S. A. A. Azeem, M. Jameel, M. Abouhawwash, Kepler optimization algorithm: A new metaheuristic algorithm inspired by kepler's laws of planetary motion, *Knowledge-Based Systems* 268 (2023) 110454.

- [18] S. Li, W. Gong, Q. Gu, A comprehensive survey on meta-heuristic algorithms for parameter extraction of photovoltaic models, *Renewable Sustainable Energy Rev.* 141 (2021) 110828.
- [19] B. Yang, J. Wang, X. Zhang, T. Yu, W. Yao, H. Shu, F. Zeng, L. Sun, Comprehensive overview of meta-heuristic algorithm applications on pv cell parameter identification, *Energy Convers. Manage.* 208 (2020) 112595.
- [20] D. Wolpert, W. Macready, No free lunch theorems for optimization, *IEEE Trans. Evol. Comput.* 1 (1997) 67–82.
- [21] R. Saive, S-shaped current–voltage characteristics in solar cells: A review, *IEEE J. Photovolt.* 9 (2019) 1477–1484.
- [22] P. J. Roland, K. P. Bhandari, R. J. Ellingson, Electronic circuit model for evaluating S-kink distorted current-voltage curves, in: 2016 IEEE 43rd Photovoltaic Specialists Conference (PVSC), pp. 3091–3094.
- [23] A. Gaur, P. Kumar, An improved circuit model for polymer solar cells, *Prog. Photovoltaics Res. Appl.* 22 (2014) 937–948.
- [24] V.-H. Tran, R. B. Ambade, S. B. Ambade, S.-H. Lee, I.-H. Lee, Low-temperature solution-processed sno<sub>2</sub> nanoparticles as a cathode buffer layer for inverted organic solar cells, *ACS Appl Mater Interfaces* 9 (2017) 1645–1653.
- [25] G. Lastra, V. S. Balderrama, L. Reséndiz, J. Pallarès, L. F. Marsal, V. Cabrera, M. Estrada, Air environment degradation of a high-performance inverted ptb7-th:pc70bm solar cell, *IEEE J. Photovolt.* 9 (2019) 464–468.
- [26] F. Xu, J. Zhu, R. Cao, S. Ge, W. Wang, H. Xu, R. Xu, Y. Wu, M. Gao, Z. Ma, F. Hong, Z. Jiang, Elucidating the evolution of the current-voltage characteristics of planar organometal halide perovskite solar cells to an S-shape at low temperature, *Sol. Energ. Mat. Sol.* 157 (2016) 981–988.
- [27] J. Gao, J. M. Luther, O. E. Semonin, R. J. Ellingson, A. J. Nozik, M. C. Beard, Quantum dot size dependent J-V characteristics in heterojunction ZnO/PbS quantum dot solar cells, *Nano Lett.* 11 (2011) 1002–1008.
- [28] F. Yu, G. Huang, W. Lin, C. Xu, W. Deng, X. Ma, J. Huang, Lumped-parameter equivalent circuit modeling of solar cells with S-shaped i-v characteristics, *Solid-State Electron.* 156 (2019) 79–86.
- [29] E. Veinberg-Vidal, C. Dupré, P. Garcia-Linares, C. Jany, R. Thibon, T. Card, T. Salvetat, P. Scheiblin, C. Brughera, F. Fournel, Y. Desieres, Y. Veschetto, V. Sanzone, P. Mur, J. Decobert, A. Datas, Manufacturing and characterization of iii-v on silicon multijunction solar cells, *Energy Procedia* 92 (2016) 242–247.
- [30] B. Romero, G. del Pozo, B. Arredondo, D. Martín-Martín, M. P. R. Gordoa, A. Pickering, A. Pérez-Rodríguez, E. Barrena, F. J. García-Sánchez, S-shaped  $I - V$  characteristics of organic solar cells: Solving mazhari's lumped-parameter equivalent circuit model, *IEEE Trans. Electron Devices* 64 (2017) 4622–4627.
- [31] B. Y. Finck, B. J. Schwartz, Understanding the origin of the S-curve in conjugated polymer/fullerene photovoltaics from drift-diffusion simulations, *Appl. Phys. Lett.* 103 (2013) 053306.
- [32] D. S. Pillai, B. Sahoo, J. P. Ram, A. Laudani, N. Rajasekar, N. Sudhakar, Modelling of organic photovoltaic cells based on an improved reverse double diode model, *Energy Procedia* 117 (2017) 1054–1061.
- [33] B. Mazhari, An improved solar cell circuit model for organic solar cells, *Sol. Energ. Mat. Sol.* 90 (2006) 1021–1033.
- [34] F. Yu, G. Huang, W. Lin, C. Xu, An analysis for S-shaped I-V characteristics of organic solar cells using lumped-parameter equivalent circuit model, *Sol. Energy* 177 (2019) 229–240.
- [35] L. Zuo, J. Yao, H. Li, H. Chen, Assessing the origin of the S-shaped I-V curve in organic solar cells: An improved equivalent circuit model, *Sol. Energ. Mat. Sol.* 122 (2014) 88–93.
- [36] F. A. de Castro, J. Heier, F. A. Nüesch, R. Hany, Origin of the kink in current-density versus voltage curves and efficiency enhancement of polymer-C<sub>60</sub> heterojunction solar cells, *IEEE J. Sel. Top. Quantum Electron.* 16 (2010) 1690–1699.
- [37] F. J. García-Sánchez, D. Lugo-Muñoz, J. Muci, A. Ortiz-Conde, Lumped parameter modeling of organic solar cells' S-shaped I-V characteristics, *IEEE J. Photovolt.* 3 (2013) 330–335.
- [38] F. De Castro, A. Laudani, F. Riganti Fulginei, A. Salvini, An in-depth analysis of the modelling of organic solar cells using multiple-diode circuits, *Sol. Energy* 135 (2016) 590–597.
- [39] E. Sesa, D. Darwisi, X. Zhou, W. J. Belcher, P. C. Dastoor, Experimental determination of the relationship between the elements of a back-to-back diode model for organic photovoltaic cells' S-shaped I-V characteristics and cell structure, *AIP Adv.* 9 (2019) 025014.
- [40] F. J. García-Sánchez, B. Romero, Equivalent circuit models for next generation photovoltaic devices with S-shaped I-V curves, in: 2019 8th International Symposium on Next Generation Electronics (ISNE), pp. 1–4.
- [41] F. J. García-Sánchez, B. Romero, D. Lugo-Muñoz, G. del Pozo, B. Arredondo, J. J. Liou, A. Ortiz-Conde, Modelling solar cell S-shaped IV characteristics with dc lumped-parameter equivalent circuit - a review, *Facta universitatis. Series electronics and energetics* 30 (2017) 327–350.
- [42] J. Dakin, R. Brown (Eds.), *Handbook of Optoelectronics: Enabling Technologies* (Volume Two), CRC Press., 2nd edition, 2017.
- [43] B. Arredondo, B. Romero, M. Beliatis, G. del Pozo, D. Martín-Martín, J. Blakesley, G. Dibb, F. Krebs, S. Gevorgyan, F. Castro, Analysing impact of oxygen and water exposure on roll-coated organic solar cell performance using impedance spectroscopy, *Sol. Energ. Mat. Sol.* 176 (2018) 397–404.
- [44] G. del Pozo, B. Romero, B. Arredondo, Evolution with annealing of solar cell parameters modeling the s-shape of the current–voltage characteristic, *Sol. Energ. Mat. Sol.* 104 (2012) 81–86.
- [45] D. Brenes-Badiilla, D. J. Coutinho, D. R. B. Amorim, R. M. Faria, M. C. Salvadori, Reversing an S-kink effect caused by interface degradation in organic solar cells through gold ion implantation in the PEDOT:PSS layer, *J. Appl. Phys.* 123 (2018) 155502.
- [46] K. Tada, Parameter extraction from S-shaped current–voltage characteristics in organic photocell with opposed two-diode model: Effects of ideality factors and series resistance, *Phys. Status Solidi A* 212 (2015) 1731–1734.
- [47] M. Makha, P. Schwaller, K. Strassle, S. B. Anantharaman, F. Nüesch, R. Hany, J. Heier, Insights into photovoltaic properties of ternary organic solar cells from phase diagrams, *Sci. Technol. Adv. Mater.* 19 (2018) 669–682.
- [48] G. Verkhogliadov, A. Mahmoodpoor, P. Voroshilov, R. Haroldson, M. Alahbakhshi, A. G. Nasibulin, S. V. Makarov, A. A. Zakhidov, Photoinduced self-gating of perovskite photovoltaic cells in ionic liquid, *ACS Materials Au* 0 (2023) null.
- [49] A. Mahmoodpoor, G. Verkhogliadov, R. Melnikov, D. S. Saranin, P. M. Voroshilov, D. Saporin, R. Haroldson, A. G. Nasibulin, A. R. Ishteev, V. Ulyantsev, S. V. Makarov, A. A. Zakhidov, Ionic liquid gating in perovskite solar cells with fullerene/carbon nanotube collectors, *Energy*

Technology 10 (2022) 2200485.

- [50] B. Romero, G. del Pozo, B. Arredondo, Exact analytical solution of a two diode circuit model for organic solar cells showing S-shape using Lambert W-functions, *Sol. Energy* 86 (2012) 3026–3029.
- [51] K. Roberts, S. R. Valluri, On calculating the current-voltage characteristic of multi-diode models for organic solar cells, 2015.
- [52] L. Lóczsi, Guaranteed- and high-precision evaluation of the Lambert W function, *Appl. Math. Comput.* 433 (2022) 127406.
- [53] K. Tada, Bayesian estimation of equivalent circuit parameters of photovoltaic cell with S-shaped current–voltage characteristic, *Phys. Status Solidi A* 218 (2021) 2100403.
- [54] S. M. Sze, *Semiconductor Devices: Physics and Technology*, John Wiley & Sons, Inc, New York, third edition, 2012.
- [55] S. Kondratenko, V. Lysenko, Y. V. Gomeniuk, O. Kondratenko, Y. Kozyrev, O. Selyshchev, V. Dzhagan, D. R. T. Zahn, Charge carrier transport, trapping, and recombination in pedot:pss/n-si solar cells, *ACS Appl. Energy Mater.* 2 (2019) 5983–5991.
- [56] M. A. Green, General temperature dependence of solar cell performance and implications for device modelling, *Prog. Photovoltaics Res. Appl.* 11 (2003) 333–340.
- [57] R. Eberle, A. Fell, F. Schindler, J. Shahid, M. C. Schubert, Breakdown of temperature sensitivity of silicon solar cells by simulation input parameters, *Sol. Energ. Mat. Sol.* 219 (2021) 110836.
- [58] H. Ibrahim, N. Anani, Variations of PV module parameters with irradiance and temperature, *Energy Procedia* 134 (2017) 276–285.
- [59] F. Bradascaia, M. C. Cavalcanti, A. J. do Nascimento, E. A. da Silva, G. M. de Souza Azevedo, Parameter identification for PV modules based on an environment-dependent double-diode model, *IEEE J. Photovolt.* 9 (2019) 1388–1397.
- [60] A. H. Tuan Le, R. Basnet, D. Yan, W. Chen, N. Nandakumar, S. Duttagupta, J. P. Seif, Z. Hameiri, Temperature-dependent performance of silicon solar cells with polysilicon passivating contacts, *Sol. Energ. Mat. Sol.* 225 (2021) 111020.
- [61] O. Dupré, R. Vaillon, M. A. Green, Experimental assessment of temperature coefficient theories for silicon solar cells, *IEEE J. Photovolt.* 6 (2016) 56–60.
- [62] Y. Riesen, M. Stuckelberger, F.-J. Haug, C. Ballif, N. Wyrtsch, Temperature dependence of hydrogenated amorphous silicon solar cell performances, *J. Appl. Phys.* 119 (2016) 044505.
- [63] A. Rana, A. Kumar, S. Chand, R. K. Singh, Exploring deep defect state impact on open circuit voltage of conventional and inverted organic solar cells, *J. Appl. Phys.* 124 (2018) 103101.
- [64] M. Braik, A. Hammouri, J. Atwan, M. A. Al-Betar, M. A. Awadallah, White shark optimizer: A novel bio-inspired meta-heuristic algorithm for global optimization problems, *Knowledge-Based Systems* 243 (2022) 108457.
- [65] J.-S. Pan, L.-G. Zhang, R.-B. Wang, V. Snášel, S.-C. Chu, Gannet optimization algorithm : A new metaheuristic algorithm for solving engineering optimization problems, *Math. Comput. Simulation* 202 (2022) 343–373.
- [66] S. Zhao, T. Zhang, S. Ma, M. Chen, Dandelion optimizer: A nature-inspired metaheuristic algorithm for engineering applications, *Eng. Appl. Artif. Intell.* 114 (2022) 105075.
- [67] K. Wang, M. Ye, Parameter determination of Schottky–barrier diode model using differential evolution, *Solid-State Electron.* 53 (2009) 234–240.
- [68] K. Ishaque, Z. Salam, H. Taheri, A. Shamsudin, A critical evaluation of ea computational methods for photovoltaic cell parameter extraction based on two diode model, *Solar Energy* 85 (2011) 1768–1779.
- [69] Q. Huang, K. Zhang, J. Song, Y. Zhang, J. Shi, Adaptive differential evolution with a lagrange interpolation argument algorithm, *Inform. Sci.* 472 (2019) 180–202.
- [70] M. Tian, X. Gao, Differential evolution with neighborhood-based adaptive evolution mechanism for numerical optimization, *Inform. Sci.* 478 (2019) 422–448.
- [71] R. Tanabe, A. S. Fukunaga, Improving the search performance of shade using linear population size reduction, in: 2014 IEEE Congress on Evolutionary Computation (CEC), pp. 1658–1665.
- [72] A. W. Mohamed, A. A. Hadi, K. M. Jambi, Novel mutation strategy for enhancing SHADE and LSHADE algorithms for global numerical optimization, *Swarm Evol. Comput.* 50 (2019) 100455.
- [73] M. Ye, X. Wang, Y. Xu, Parameter extraction of solar cells using particle swarm optimization, *J. Appl. Phys.* 105 (2009) 094502.
- [74] N. Karaboga, S. Kockanat, H. Dogan, The parameter extraction of the thermally annealed schottky barrier diode using the modified artificial bee colony, *Appl. Intell.* 38 (2013) 279–288.
- [75] S. Mirjalili, A. Lewis, The whale optimization algorithm, *Adv. Eng. Software* 95 (2016) 51–67.
- [76] D. Oliva, M. Abd El Aziz, A. Ella Hassani, Parameter estimation of photovoltaic cells using an improved chaotic whale optimization algorithm, *Appl. Energy* 200 (2017) 141–154.
- [77] A. Sadollah, H. Sayyaadi, A. Yadav, A dynamic metaheuristic optimization model inspired by biological nervous systems: Neural network algorithm, *Appl. Soft Comput.* 71 (2018) 747–782.
- [78] S. J. Patel, A. K. Panchal, V. Kheraj, Extraction of solar cell parameters from a single current–voltage characteristic using teaching learning based optimization algorithm, *Appl. Energy* 119 (2014) 384–393.
- [79] X. Chen, K. Yu, W. Du, W. Zhao, G. Liu, Parameters identification of solar cell models using generalized oppositional teaching learning based optimization, *Energy* 99 (2016) 170–180.
- [80] Q. Niu, H. Zhang, K. Li, An improved TLBO with elite strategy for parameters identification of PEM fuel cell and solar cell models, *Int. J. Hydrogen Energy* 39 (2014) 3837–3854.
- [81] R. M. May, Simple mathematical models with very complicated dynamics, *Nature* 261 (1976) 459–467.
- [82] Y.-J. Zheng, Water wave optimization: A new nature-inspired metaheuristic, *Comput. Oper. Res.* 55 (2015) 1–11.
- [83] R. Rao, Jaya: A simple and new optimization algorithm for solving constrained and unconstrained optimization problems, *International Journal of Industrial Engineering Computations* 7 (2016) 19–34.
- [84] K. Yu, J. Liang, B. Qu, X. Chen, H. Wang, Parameters identification of photovoltaic models using an improved JAYA optimization algorithm, *Energy Convers. Manage.* 150 (2017) 742–753.

- [85] S. Mirjalili, SCA: A sine cosine algorithm for solving optimization problems, *Knowledge-Based Systems* 96 (2016) 120–133.
- [86] W. Long, T. Wu, X. Liang, S. Xu, Solving high-dimensional global optimization problems using an improved sine cosine algorithm, *Expert Syst. Appl.* 123 (2019) 108–126.
- [87] S. Gupta, K. Deep, A hybrid self-adaptive sine cosine algorithm with opposition based learning, *Expert Syst. Appl.* 119 (2019) 210–230.
- [88] P. P. Biswas, P. Suganthan, G. Wu, G. A. Amaralunga, Parameter estimation of solar cells using datasheet information with the application of an adaptive differential evolution algorithm, *Renew. Energ.* 132 (2019) 425–438.
- [89] J. Derrac, S. García, D. Molina, F. Herrera, A practical tutorial on the use of nonparametric statistical tests as a methodology for comparing evolutionary and swarm intelligence algorithms, *Swarm Evol. Comput.* 1 (2011) 3–18.
- [90] V. Sahargahi, V. Majidnezhad, S. T. Afshord, Y. Jafari, An intelligent chaotic clonal optimizer, *Appl. Soft Comput.* 115 (2022) 108126.

**Table 4**

Adjusted *p*-values for tests for  $N \times N$  multiple comparisons of  $I_{01}$  estimation among all methods in the single-IV case ( $p < 1.0$  are only shown).

Hypothesis	Nemenyi	post-hoc procedure	
		Holm	Shaffer
ADELI versus WW	<1E-13	<1E-13	<1E-13
ADELI versus NDE	1.17195E-12	1.15907E-12	1.00453E-12
STLBO versus CWOA	1.17195E-12	1.15907E-12	1.00453E-12
TLBO versus PSO	1.21236E-12	1.17240E-12	1.03917E-12
STLBO versus GOTLBO	1.21236E-12	1.17240E-12	1.03917E-12
ADELI versus DE	1.73772E-12	1.64224E-12	1.48948E-12
STLBO versus DE	1.83875E-12	1.71752E-12	1.57607E-12
ADELI versus CWOA	3.83915E-12	3.50164E-12	3.29070E-12
EBLSHADE versus GOTLBO	4.20286E-12	3.78719E-12	3.60245E-12
STLBO versus NDE	5.01110E-12	4.46043E-12	4.29523E-12
ADELI versus GOTLBO	5.41522E-12	4.76064E-12	4.64162E-12
EBLSHADE versus CWOA	5.98099E-12	5.19229E-12	5.12657E-12
EBLSHADE versus ISCA	1.17195E-11	1.00453E-11	1.00453E-11
EBLSHADE versus DE	1.45282E-11	1.22931E-11	1.06966E-11
EBLSHADE versus NDE	4.17053E-11	3.43725E-11	3.07061E-11
STLBO versus ISCA	8.17133E-11	6.64482E-11	6.01625E-11
TLBO versus WW	8.82197E-11	7.07696E-11	6.49529E-11
TLBO versus MABC	1.07900E-10	8.53717E-11	7.94431E-11
EBLSHADE versus MABC	3.09961E-10	2.38431E-10	2.28213E-10
ADELI versus NNA	3.24570E-10	2.46102E-10	2.38969E-10
ADELI versus ISCA	3.83410E-10	2.86504E-10	2.82291E-10
STLBO versus MABC	1.58351E-09	1.16588E-09	1.16588E-09
STLBO versus NNA	1.83408E-09	1.33021E-09	1.33021E-09
TLBO versus ISCA	3.49326E-09	2.49519E-09	2.22648E-09
ADELI versus MABC	5.83612E-09	4.10452E-09	3.71972E-09
EBLSHADE versus NNA	1.23520E-08	8.55140E-09	7.87272E-09
EBLSHADE versus PSO	1.47150E-08	1.00256E-08	9.37877E-09
STLBO versus PSO	5.32586E-08	3.57008E-08	3.39450E-08
ADELI versus PSO	1.50038E-07	9.89261E-08	.56286E-08
TLBO versus GOTLBO	2.16253E-07	1.40208E-07	1.37831E-07
EBLSHADE versus WW	2.39169E-07	1.52438E-07	1.52438E-07
TLBO versus CWOA	2.89034E-07	1.81043E-07	1.77867E-07
TLBO versus DE	5.91345E-07	3.63905E-07	3.63905E-07
STLBO versus WW	6.86296E-07	4.14794E-07	4.14794E-07
TLBO versus NDE	1.37158E-06	8.13904E-07	7.68687E-07
TLBO versus NNA	1.17758E-04	6.72904E-05	6.59964E-05
NNA versus WW	2.21281E-02	1.24015E-02	1.24015E-02
IJAYA versus WW	2.36193E-01	1.29777E-01	1.24585E-01
NNA versus PSO	2.36193E-01	1.29777E-01	1.24585E-01
NDE versus WW	4.04596E-01	2.13413E-01	2.13413E-01
DE versus WW	6.28685E-01	3.24706E-01	3.24706E-01
CWOA versus WW	8.94683E-01	4.52257E-01	4.52257E-01
GOTLBO versus WW	1.0	5.07626E-01	5.07626E-01
IJAYA versus PSO	1.0	8.15876E-01	7.97333E-01
NNA versus MABC	1.0	9.64793E-01	9.64793E-01

**Table 5**

The total count of wins and losses for each algorithm in  $N \times N$  multiple comparisons using the Friedman test and Shaffer's static, Nememyi, and Holm post-hoc procedures in single-IV case. The criterion for victory was a adjusted  $p$ -value less than 0.1.

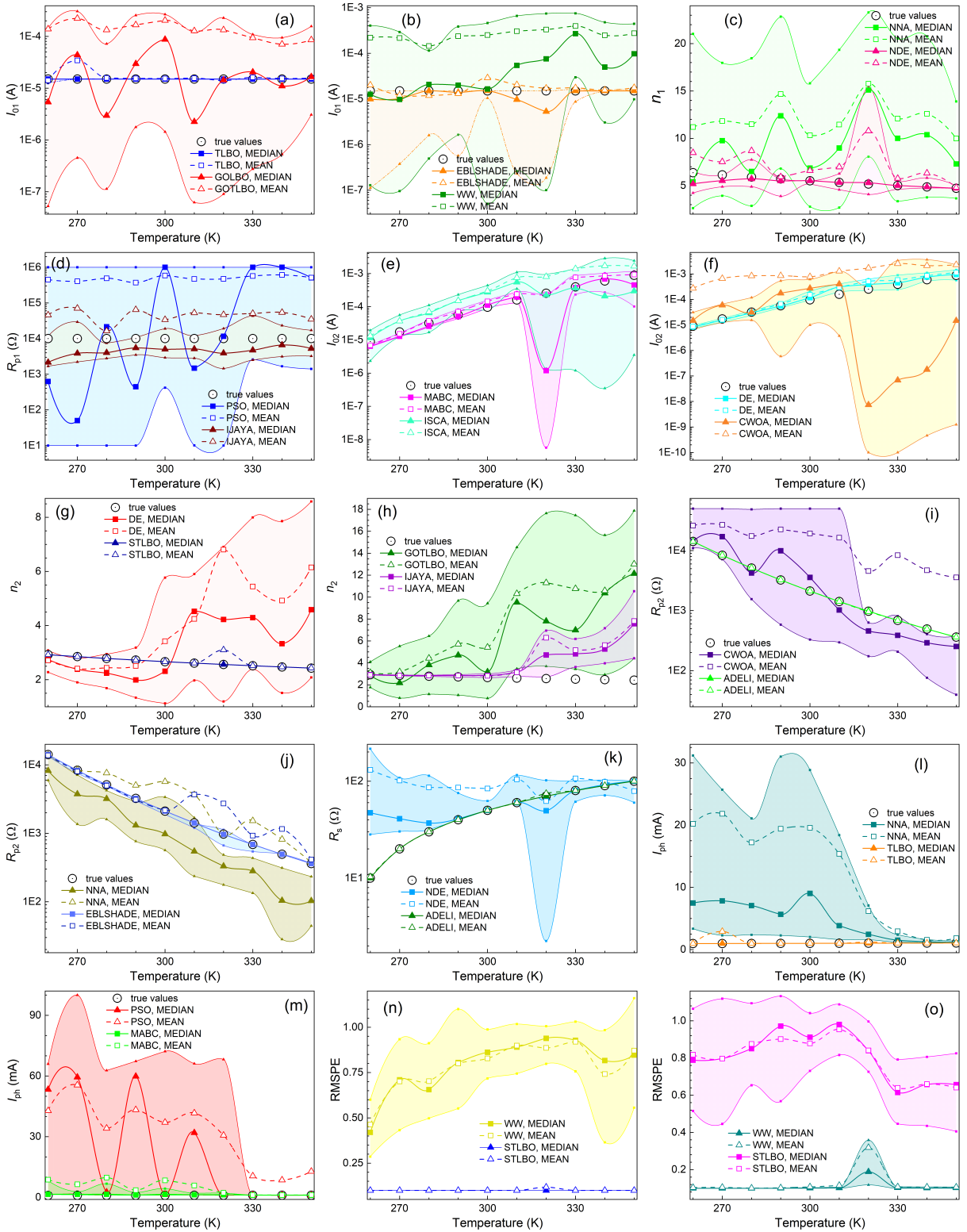
Algorithm	Wins / Loses										Total
	task										
$I_{01}$	$n_1$	$R_{p1}$	$I_{02}$	$n_2$	$R_{p2}$	$R_s$	$I_{ph}$	RMSPE	Comp		
DE	0/12	17/12	17/12	0/12	12/12	14/12	5/12	17/12	15/15	0/0	97/111
EBLSHADE	27/0	27/0	27/0	27/0	27/0	27/0	27/0	27/0	26/0	21/0	<b>263/0</b>
ADELI	27/0	27/0	27/0	27/0	27/0	27/0	27/0	27/0	27/0	14/0	<b>257/0</b>
NDE	0/12	21/12	18/11	3/12	18/9	3/12	18/11	21/9	24/8	0/0	126/96
MABC	0/12	0/15	10/12	0/12	11/12	0/17	3/12	2/15	12/15	0/3	38/125
TLBO	27/0	27/0	26/0	27/0	24/0	27/0	26/0	24/0	24/0	10/0	242/0
GOTLBO	0/12	0/18	0/24	0/12	3/15	0/12	3/15	0/21	0/21	0/5	6/155
STLBO	27/0	27/0	27/0	27/0	27/0	27/0	27/0	27/0	27/0	11/0	<b>254/0</b>
PSO	0/12	0/21	0/24	0/15	0/24	0/21	0/34	0/23	0/18	0/12	0/204
IJAYA	0/0	16/0	18/0	0/0	12/0	11/0	3/0	18/0	18/0	0/0	<b>96/0</b>
ISCA	0/12	0/21	0/23	0/12	3/15	0/12	2/15	0/21	0/24	0/3	5/158
NNA	3/12	0/21	0/23	0/12	0/23	0/14	0/17	0/21	0/24	0/9	3/176
CWOA	0/12	0/21	0/21	0/12	0/24	0/18	3/15	0/21	0/24	0/12	3/180
WW	0/15	0/21	0/20	0/12	0/30	0/18	2/15	0/20	0/24	0/12	2/187

**Table 6**

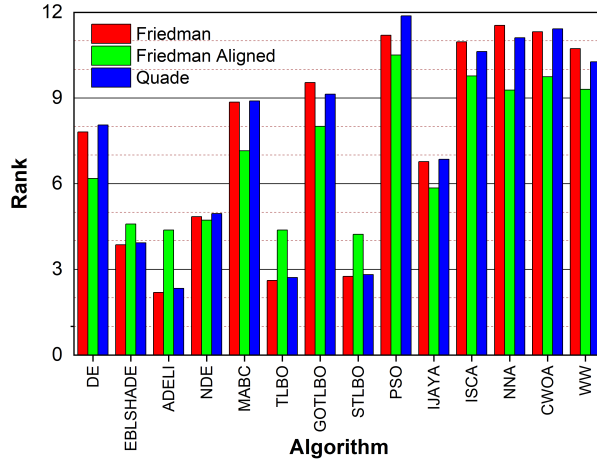
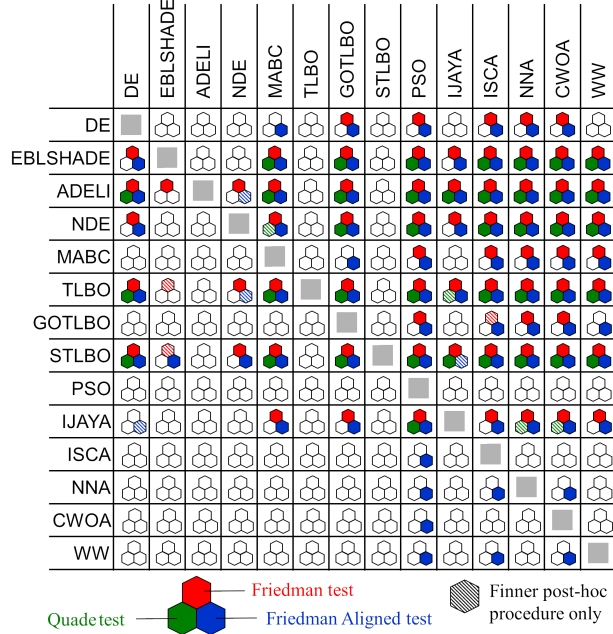
The results of Wilcoxon signed-rank test with a level of significance  $\alpha = 0.05$  in the IV-set case. The “+” indicated that the null hypothesis was rejected, and the control algorithm (in the row) performed better then the comparison algorithm (in the column). The “0” indicates to rejection of the hypothesis about outperforming the control algorithm.

Control algorithm	Comparison algorithm											Total			
	DE	EBLSHADE	ADELI	NDE	MABC	TLBO	GOTLBO	STLBO	PSO	IJAYA	ISCA	NNA	CWOA	WW	(+/-)
DE	■	0	0	0	+	0	+	0	+	0	+	+	+	+	7/0/6
EBLSHADE	+	■	0	+	+	0	+	0	+	+	+	+	+	+	10/0/3
ADELI	+	+	■	+	+	+	+	+	+	+	+	+	+	+	13/0/0
NDE	+	0	0	■	+	0	+	0	+	+	+	+	+	+	9/0/4
MABC	0	0	0	0	■	0	+	0	+	0	+	+	+	+	6/0/7
TLBO	+	+	0	+	+	■	+	0	+	+	+	+	+	+	11/1/1
GOTLBO	0	0	0	0	0	0	■	0	+	0	+	+	+	+	5/0/8
STLBO	+	+	0	+	+	0	+	■	+	+	+	+	+	+	11/1/1
PSO	0	0	0	0	0	0	0	■	0	0	0	0	0	0	0/4/9
IJAYA	+	0	0	0	+	0	+	0	+	■	+	+	+	+	8/0/5
ISCA	0	0	0	0	0	0	0	0	0	0	■	0	0	0	0/3/10
NNA	0	0	0	0	0	0	0	0	0	0	0	■	0	0	0/3/10
CWOA	0	0	0	0	0	0	0	0	0	0	0	■	0	0	0/4/9
WW	0	0	0	0	0	0	0	0	0	0	0	+	0	■	1/3/9

## Meta-heuristic parameter extraction of SCs with S-shaped IV curves



**Figure 9:** Dependences of the  $I_{01}$  (a, b),  $n_1$  (c),  $R_{p1}$  (d),  $I_{02}$  (e, f),  $n_2$  (g, h),  $R_{p2}$  (i, j),  $R_s$  (k),  $I_{ph}$  (l, m), and RMSPE (n, o) estimation by different algorithm on the synthesis temperature. The IV-set is used. The circles represent the values, which have been used in IV curve simulations, the filled marks represent the median values, and the empty marks represent the mean values. The colored regions correspond to the IQR. The lines only serve as guide to the eye.

**Figure 10:** Ranking of the algorithms according to Friedman, Friedman Aligned, and Quade tests in the IV-set case.**Figure 11:** The results of algorithm  $1 \times N$  comparisons by Friedman, Friedman Aligned, and Quade tests in the IV-set case. The colored hexagon indicates that the adjusted  $p$ -value, which tests the hypothesis that an algorithm in a row outperforms the algorithm in a column, is not greater than  $p_{cr} = 0.1$ . The solid fill signifies that every post-hoc procedure resulted in  $p < p_{cr}$ ; the dashed fill indicates that the Finner post-hoc procedure was the only method that produced this result. The correspondence between the color and position of the hexagon to a test is shown in a legend at the bottom of the figure.

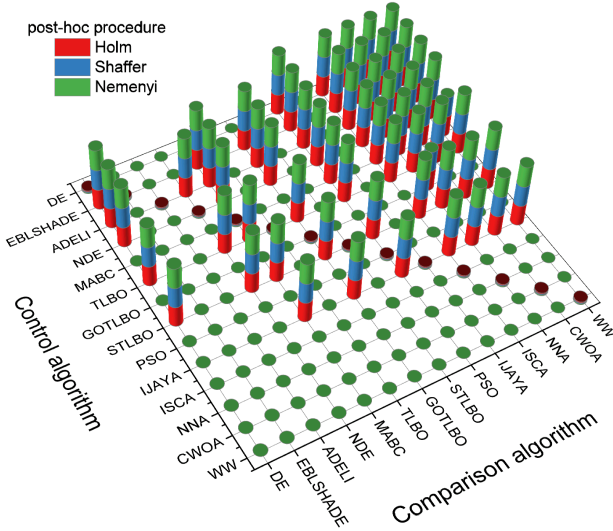


**Figure 12:** The results of multiple comparisons among all algorithms in the IV-set case. The colored cylinder indicates that the adjusted p-value, which tests the control algorithm outperforms the comparison algorithm, is not greater than  $p_{cr} = 0.1$ . The correspondence between the color of the cylinder to a post-hoc procedure is shown in the figure's legend.

**Table 7**

The total count of wins and losses for each algorithm in  $1 \times N$  and  $N \times N$  multiple comparisons using the all tests and post-hoc procedures in the IV-set case. The criterion for victory was a adjusted p-value less than 0.1. The best results are bolded.

Algorithm	Wins / Loses	
	$1 \times N$ comparisons	$N \times N$ comparisons
DE	44/53	15/15
EBLSHADE	100/6	24/ <b>0</b>
ADELI	<b>117/0</b>	<b>27/0</b>
NDE	97/18	24/9
MABC	44/69	14/18
TLBO	<b>111/0</b>	<b>27/0</b>
GOTLBO	25/80	2/18
STLBO	<b>118/0</b>	<b>27/0</b>
PSO	0/112	0/24
IJAYA	63/46	21/ <b>0</b>
ISCA	4/97	0/24
NNA	12/93	0/26
CWOA	4/101	0/24
WW	12/80	0/23